MIT Libraries | DSpace@MIT

MIT Open Access Articles

A surface mesh smoothing and untangling method independent of the CAD parameterization

The MIT Faculty has made this article openly available. ***Please share*** how this access benefits you. Your story matters.

Citation: Gargallo-Peiró, Abel, Xevi Roca, and Josep Sarrate. "A Surface Mesh Smoothing and Untangling Method Independent of the CAD Parameterization." Comput Mech 53, no. 4 (September 11, 2013): 587–609.

As Published: http://dx.doi.org/10.1007/s00466-013-0920-1

Publisher: Springer Berlin Heidelberg

Persistent URL: http://hdl.handle.net/1721.1/107382

Version: Author's final manuscript: final author's manuscript post peer review, without publisher's formatting or copy editing

Terms of Use: Article is made available in accordance with the publisher's policy and may be subject to US copyright law. Please refer to the publisher's site for terms of use.

Massachusetts Institute of Technology

Noname manuscript No.
(will be inserted by the editor)

A surface mesh smoothing and untangling method independent of the CAD parameterization

Abel Gargallo-Peiró · Xevi Roca · Josep Sarrate

Received: date / Accepted: date

Abstract A method to optimize triangular and quadrilateral meshes on parameterized surfaces is proposed. The optimization procedure relocates the nodes on the surface to improve the quality (smooth) and ensures that the elements are not inverted (untangle). We detail how to express any measure for planar elements in terms of the parametric coordinates of the nodes. The extended measures can be used to check the quality and validity of a surface mesh. Then, we detail how to optimize any Jacobian-based distortion measure to obtain smoothed and untangled meshes with the nodes on the surface. We prove that this method is independent of the surface parameterization. Thus, it can optimize meshes on CAD surfaces defined by low-quality parameterizations. The examples show that the method can optimize meshes composed by a large number of inverted elements. Finally, the method can be extended to obtain high-order meshes with the nodes on the CAD surfaces.

Keywords mesh quality; mesh optimization; smoothing and untangling; CAD surfaces;

1 Introduction

In the last decades, unstructured methods such as the Finite Element Method, the Finite Volume Method, and the Discontinuous Galerkin Method have shown to be powerful tools to simulate natural phenomena in applied sciences and engineering. The main advantage of unstructured methods compared to structured methods, such as the finite differences, is the geometrical flexibility. That is, unstructured methods can be applied to complex and arbitrary three-dimensional domains. To this end, one has to generate first a mesh of the domain composed by polyhedra, such as tetrahedral or hexahedral elements. In addition, the mesh has to be composed by non-inverted elements (valid) with a shape close to an ideal element (quality) [7,17,19]. On the one hand, if at least one element that composes the discretization of the domain is inverted, the variational formulation for that mesh is not valid, and the unstructured method cannot be applied. On the other hand, just a few low-quality elements can compromise the accuracy of the solution in the whole domain.

The standard technique to improve the quality of a mesh is referred as smoothing [15,13,20]. This technique improves the quality of an initial mesh by relocating the nodes without modifying the mesh topology. However, some smoothing methods can lead to final meshes that contain inverted elements. This issue is usually triggered when the mesh boundary contains non-convex features. Moreover, if the initial mesh contains inverted elements, few smoothing methods can repair them (untangle) and therefore, the final mesh is not valid. To address this issue, there are several methods specialized to untangle the mesh [9,18,8]. Note that combining an untangling method with a smoothing technique, we can obtain the desired valid and high-quality mesh [6].

The application of a node relocation technique requires to consider two types of nodes, the ones on the interior and those on the boundary. In three-dimensional

A. Gargallo-Peiró and J. Sarrate
Laboratori de Càlcul Numèric (LaCàN), Departament de Matemàtica Aplicada III, Universitat Politècnica de Catalunya, Jordi Girona 1, E-08034 Barcelona, Spain. E-mail: abel.gargallo@upc.edu, jose.sarrate@upc.edu

X. Roca
Aeronautics and Astronautics, Massachusetts Institute of Technology, Cambridge, MA 02139, USA. E-mail: xeviroca@mit.edu

meshes, the interior nodes can move freely inside their container volumes (three degrees of freedom), while the boundary nodes can only move on their container surfaces (two degrees of freedom). Note that, an inverted or low-quality face (triangle / quadrilateral), with the nodes on the boundary surfaces, also determines a non-valid or a low-quality volume element (tetrahedron / hexahedron). Hence, relocating the nodes on the boundary surfaces is required to ensure a valid and high-quality three-dimensional mesh. In addition, valid surface meshes are an essential ingredient to perform computational mechanics simulations with shell elements.

The formulation of a relocation technique that ensures that the nodes move on a surface depends on the surface representation. There are several computational techniques to represent a surface, such as a triangular mesh, an implicit entity, or a CAD entity. The last technique is the preferred representation for industrial applications, where CAD models have to be simulated during the design process. However, not all CAD surfaces have high-quality parameterizations where the derivative matrix is well-conditioned, non-singular, and varies smoothly. Thus, a robust relocation technique has to provide valid and high-quality meshes for both low and high-quality parameterizations.

The main contribution of this work is to develop a relocation method (constant mesh topology) that robustly untangles the elements on a given CAD surface. The method does not modify the initial surface parameterization and therefore, does not approximate the surface. Specifically, we present a simultaneous smoothing and untangling technique for linear meshes (triangles and quadrilaterals) with the nodes on a parameterized surface. This technique allows obtaining valid and high-quality linear meshes on surfaces represented by both low and high-quality CAD parameterizations. To this end, we propose:

- To extend any distortion and quality measure for linear elements to elements with the nodes on parameterized surfaces, Section 3. The resulting measures are expressed on the parametric coordinates of the element nodes. Moreover, we prove that they are independent of the surface parameterization.
- To enforce the ideal element quality by solving an optimization problem in terms of the parametric coordinates, Section 4. We prove that this formulation is independent of the surface parameterization. This property ensures that the method can be applied to optimize meshes on surfaces represented by low-quality parameterizations.

To accomplish our purposes, we also adapt and extend two existing techniques. First, to avoid the vertical asymptotes that appear in the untangling process, we use the parameter dependent modification for Jacobian-based distortions presented in [6]. Herein, we propose a new formula to automatically choose the modification parameter. Thus, the implementation of the method can smooth and untangle meshes composed by a large number of inverted elements. Second, to obtain optimized meshes that preserve a prescribed element-size field, we combine a shape and a size distortion (quality) measure as in [17]. The main difference is that the proposed measure is differentiable everywhere and therefore, can be used in the optimization process.

The rest of the paper is organized as follows. First, in Section 2 we review the related work on surface mesh optimization. In Section 3, we detail how to extend any distortion (quality) measure for linear elements to elements with the nodes on a parameterized surface. Then, we detail how to optimize the surface mesh, Section 4. Specifically, we enforce the ideal element distortion by means of a non-linear least-squares problem in terms of the parametric coordinates, Section 4.1. This can be implemented in terms of the deviation of the submesh distortion with respect to an ideal configuration, Section 4.2. This implementation of the optimization algorithm is described in Section 4.3. For completeness, in Section 4.4 we detail how to incorporate several Jacobian-based distortion measures in the optimization algorithm. In particular, we detail how to choose the parameter of the distortion measure modification. We also introduce the combined shape and size distortion (quality) measure. Finally, we present several examples to assess the properties of the proposed method, Section 5. In addition, we outline how to extend the method to obtain valid and high-quality high-order meshes on parameterized CAD surfaces. Specifically, we illustrate this extension by generating a high-order mesh on the surface of a propeller.

2 Related work

The main purpose of the quality measures is to quantify the geometric suitability of the elements of a mesh, see [7] for a comparative analysis. To this end, we use the framework of algebraic quality measures introduced by Knupp [17,19]. In this framework, the distortion (quality) measures are defined in terms of an affine mapping between an ideal element and the physical one. Specifically, the Jacobian matrix of this mapping is used to measure the deviation of the physical element with respect to the ideal one (distortion). Therefore, the value of the quality (distortion) measures is determined by the physical coordinates of the element vertices. In this work, we rewrite the expression of the Jacobian-based

quality (distortion) measure in terms of the parametric coordinates of the element vertices.

Quality measures can be also used to improve the quality of a mesh by an optimization-based procedure. In particular, Knupp proposed a smoothing method based on the optimization of Jacobian-based measures [20]. However, this type of optimization procedures does not ensure that an initial mesh with inverted elements can be untangled. To overcome this issue, Freitag proposed in [9] a mesh improving procedure divided into two steps: a linear untangling, and a maximization of the element with minimum area (volume) of the mesh. Later, similar techniques organized in two independent optimization have been proposed [18,8]. Afterwards, Escobar *et al.* [6] proposed a simultaneous smoothing and untangling technique. They also extended this technique to non-planar triangular meshes [5,4]. To perform the simultaneous untangling and smoothing, they propose a parameter dependent modification of the element distortion. In this way, they obtain a convex goal function, with a similar minimum and without the vertical asymptotes that separate the unfeasible (tangled elements) and the feasible regions (valid elements). Reference [23] uses the parameter-dependent modification presented in [6] and proposes a new optimization approach that takes as minimization variables the node coordinates and the modification parameter. In our work, we use the same modification of the element distortion than in [6]. However, we propose a different approach to determine automatically the modification parameter.

Several relocation techniques for surface meshes have been previously developed. These techniques can be classified into two groups, depending on whether the nodes are relocated indirectly or directly on a surface representation. On the one hand, indirect relocation methods compute an ideal location of the nodes. However, the resulting node locations can be off the surface. Therefore, an additional step to relocate the nodes on, or close to, the surface is required [5,4,10,16,31,32,21]. In particular, Escobar *et al.* present in [5,4] a simultaneous untangling and smoothing method for triangular surface meshes. They use, for each surface node, a local projection plane where the patch around the node is smoothed. Then, the new node location is projected back close to the original triangulation. On the other hand, direct relocation methods obtain an ideal location of the nodes on the surface. To this end, the mesh optimization is expressed in terms of the parametric coordinates of an approximated representation of the original surface [12,11,30]. In particular, Shivanna *et al.* present in [30] two methods for the smoothing and untangling of quadrilateral meshes defined on underlying triangulated surfaces. The first is based on the optimization of the mesh on local parametric spaces, and the second is based on the projection of the advancing directions on the discrete surface. We also formulate the smoothing and untangling optimization in terms of the parametric coordinates of the nodes. However, we use the original CAD representation instead of a smooth representation of an initial triangulation.

It is worth noting that in geometry processing optimization approaches have been used to reparameterize triangular surface meshes [24]. Then, the obtained parameterization can be used to remesh the discrete representation of the initial surface [1,2]. On the contrary, we use the initial continuous parameterization of the CAD surface and not a piecewise linear approximation. Moreover, our method is independent of the surface parameterization. Thus, we do not need to reparameterize to obtain a high-quality mesh on a low-quality parameterization of the initial CAD surface.

Finally, we highlight that all the reviewed smoothing and untangling methods use an approximated representation of the geometry of the model. On the contrary, our method uses the initial CAD representation of the geometry regardless of the quality of its parameterization. Note that a smoothing and untangling approach that deals with the exact CAD representation and it is proved to be independent of the parameterization has not been proposed before.

3 Distortion and quality for elements on parameterized surfaces

In this section, we first develop an analytical formulation to extend any quality measure for planar triangles to triangular meshes on a parameterized surface. As a result, we obtain a quality measure expressed in the two coordinates of the parametric space of the surface. Then, we develop the formulation for quadrilateral elements expressing it in terms of the formulation for triangles.

Note that triangle elements on a surface are two-dimensional planar entities immersed in $\mathbb{R}^3$. Hence, a possible approach to qualify surface elements is to use planar quality measures in the plane where the surface element lies. However, this approach does not allow a straight forward surface optimization procedure. Parameterized surfaces enable the development of an analytical and straightforward function to quantify the quality of a surface triangular element. Herein, we propose a composition of the parameterization of the surface together with a mapping of the surface element to a similar one in a 2D space, where planar quality measures are defined. This way, the proposed quality is expressed

in terms of the parametric coordinates of the surface. Such expression allows a natural smoothing technique that avoids any additional constraint to keep the nodes on the surface, since the procedure is developed on its parametric space.

3.1 Preliminaries

Let η be a distortion measure for planar elements, with image $[1, \infty)$, taking value 1 for an ideal configuration of the element, and value ∞ when it is degenerated or tangled. Let q be the corresponding quality measure, defined as

$$q = \frac{1}{\eta}. \tag{1}$$

The image of the quality measure q is $[0, 1]$, taking value 1 for ideal configurations and 0 for degenerated or tangled ones.

Given a distortion and its associated quality measure for triangles in the plane, our goal is to extend these measure to triangles with the vertices on a parameterized surface, Σ. Assume that the surface Σ is parameterized by a continuously differentiable and globally invertible mapping

$$\begin{aligned} \varphi : \ & \mathcal{U} \subset \mathbb{R}^2 \ \longrightarrow \ \Sigma \subset \mathbb{R}^3 \\ & \mathbf{u} = (u, v) \longmapsto \mathbf{x} = \varphi(\mathbf{u}). \end{aligned} \tag{2}$$

Through this work, we require that the nodes of the triangles lie on the proper spaces. To this end, we introduce the definition of the following triangle sets:

- The set of triangles with vertices on $\Sigma \subset \mathbb{R}^3$:

$$\mathcal{T}_\Sigma := \{t_\Sigma = (\mathbf{x}_0, \mathbf{x}_1, \mathbf{x}_2) \in \Sigma \times \Sigma \times \Sigma \subset \mathbb{R}^3 \times \mathbb{R}^3 \times \mathbb{R}^3\}.$$

- The set of triangles in $\mathbb{R}^2$:

$$\mathcal{T} := \{t = (\mathbf{y}_0, \mathbf{y}_1, \mathbf{y}_2) \in \mathbb{R}^2 \times \mathbb{R}^2 \times \mathbb{R}^2\}.$$

- The set of triangles in the parametric space $\mathcal{U}$:

$$\mathcal{T}_\mathcal{U} := \{t_\mathcal{U} = (\mathbf{u}_0, \mathbf{u}_1, \mathbf{u}_2) \in \mathcal{U} \times \mathcal{U} \times \mathcal{U}\}.$$

Using these sets, the distortion and quality measures for planar elements presented in Equation (1) can be expressed as the mappings

$$\eta : \mathcal{T} \subset \mathbb{R}^2 \times \mathbb{R}^2 \times \mathbb{R}^2 \longrightarrow [1, \infty) \subset \mathbb{R}, \tag{3}$$

$$q : \mathcal{T} \subset \mathbb{R}^2 \times \mathbb{R}^2 \times \mathbb{R}^2 \longrightarrow [0, 1] \subset \mathbb{R}. \tag{4}$$

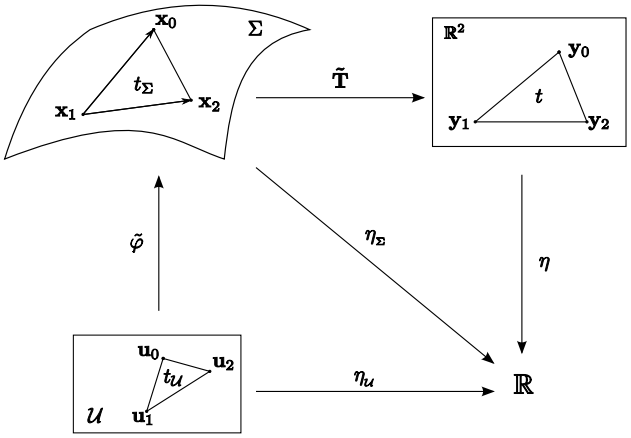

Fig. 1 Diagram of mappings involved in the definition of the quality measure.

3.2 Measures for triangles on parametric coordinates

To evaluate the quality of a triangle t_Σ with vertices on a surface Σ, we first express the vertices as the image by the parameterization φ of the corresponding parametric coordinates in $\mathcal{U}$. Since t_Σ is planar, but it is immersed in $\mathbb{R}^3$, we define the quality of the physical triangle as the quality of a geometrically equivalent triangle t on $\mathbb{R}^2$. Once in $\mathbb{R}^2$, the proposed formulation allows to extend any existing distortion and quality measure for planar elements. In Section 4.4, we detail the distortion measures considered in this work.

We first extend the surface parameterization φ to the corresponding triangle sets. To this end, we define the mapping

$$\begin{aligned} \tilde{\varphi} : \mathcal{T}_\mathcal{U} \longrightarrow & \quad \mathcal{T}_\Sigma \\ t_\mathcal{U} \longmapsto & \ t_\Sigma = (\varphi(\mathbf{u}_0), \varphi(\mathbf{u}_1), \varphi(\mathbf{u}_2)). \end{aligned} \tag{5}$$

This mapping transforms a triangle $t_\mathcal{U} = (\mathbf{u}_0, \mathbf{u}_1, \mathbf{u}_2)$ in the parametric space $\mathcal{U}$, to a triangle $t_\Sigma = (\mathbf{x}_0, \mathbf{x}_1, \mathbf{x}_2)$ with the nodes on the surface Σ determined by φ, see Figure 1. Since t_Σ defines a plane in $\mathbb{R}^3$, we can map t_Σ to a geometrically equivalent triangle in $\mathbb{R}^2$. That is, we can define a mapping $\tilde{\mathbf{T}}$ from $\mathcal{T}_\Sigma$ to $\mathcal{T}$. To define $\tilde{\mathbf{T}}$, we consider an auxiliary linear mapping $\mathbf{T}$ from $\mathbb{R}^3$ to the plane. The domain of this mapping is expressed in the canonical basis of $\mathbb{R}^3$, and the image is expressed in terms of a new 2D orthogonal basis determined by a combination of two edges of the triangle. Let

$$\mathbf{e}_1 := \mathbf{x}_2 - \mathbf{x}_1,$$

$$\mathbf{e}_2 := \mathbf{x}_0 - \mathbf{x}_1,$$

be the vectors determined by two edges of the triangle. Then, we define

$$\tilde{\mathbf{e}}_1 := \frac{\mathbf{e}_1}{\|\mathbf{e}_1\|},$$

$$\tilde{\mathbf{e}}_2 := \gamma\ \tilde{\mathbf{e}}_{2,0}, \qquad \text{with} \quad \tilde{\mathbf{e}}_{2,0} := \frac{\mathbf{e}_2 - (\mathbf{e}_2^T \cdot \tilde{\mathbf{e}}_1)\ \tilde{\mathbf{e}}_1}{\|\mathbf{e}_2 - (\mathbf{e}_2^T \cdot \tilde{\mathbf{e}}_1)\ \tilde{\mathbf{e}}_1\|},$$

as the two orthonormal vectors of the new basis, where γ is defined to ensure a well oriented orthonormal basis. Specifically, we define γ as:

$$\gamma := \frac{(\tilde{\mathbf{e}}_1 \times \tilde{\mathbf{e}}_{2,0}) \cdot \mathbf{n}}{|(\tilde{\mathbf{e}}_1 \times \tilde{\mathbf{e}}_{2,0}) \cdot \mathbf{n}|} = \frac{\det(\tilde{\mathbf{e}}_1, \tilde{\mathbf{e}}_{2,0}, \mathbf{n})}{|\det(\tilde{\mathbf{e}}_1, \tilde{\mathbf{e}}_{2,0}, \mathbf{n})|},$$

where $\mathbf{n} \equiv \mathbf{n}(\mathbf{x}_1) = \frac{\partial \varphi}{\partial u}(u_1, v_1) \times \frac{\partial \varphi}{\partial v}(u_1, v_1)$ is the normal to the surface at $\mathbf{x}_1 = \varphi(u_1, v_1)$. Note that $\gamma = \pm 1$, being 1 for counter-clockwise oriented triangles, and -1 for clockwise oriented ones. It is important to point out that if $\mathbf{e}_1$ and $\mathbf{e}_2$ are linearly dependent, we define $\tilde{\mathbf{e}}_2$ as the unitary vector orthogonal to $\tilde{\mathbf{e}}_1$ that completes a positive oriented base.

Now, we can define $\mathbf{T}$ as

$$\begin{aligned} \mathbf{T} : \mathbb{R}^3 &\longrightarrow \mathbb{R}^2 \\ \mathbf{x} &\longmapsto \mathbf{y} = \mathbf{M} \cdot (\mathbf{x} - \mathbf{x}_1), \end{aligned} \tag{6}$$

where $\mathbf{M} = (\tilde{\mathbf{e}}_1 \ \ \tilde{\mathbf{e}}_2)^T$ is a 2×3 matrix. In addition, we define $\tilde{\mathbf{T}}$ as:

$$\begin{aligned} \tilde{\mathbf{T}} : \mathcal{T}_\Sigma &\longrightarrow \mathcal{T} \\ t_\Sigma &\longmapsto t = (\mathbf{T}(\mathbf{x}_0), \mathbf{T}(\mathbf{x}_1), \mathbf{T}(\mathbf{x}_2)). \end{aligned} \tag{7}$$

Hence, we can express the distortion measure for a triangle t_Σ on the surface as:

$$\begin{aligned} \eta_\Sigma : \quad \mathcal{T}_\Sigma \quad &\xrightarrow{\tilde{\mathbf{T}}} \quad \mathcal{T} \quad \xrightarrow{\eta} \quad \mathbb{R} \\ (\mathbf{x}_0, \mathbf{x}_1, \mathbf{x}_2) &\longmapsto \tilde{\mathbf{T}}(\mathbf{x}_0, \mathbf{x}_1, \mathbf{x}_2) \longmapsto \eta(\tilde{\mathbf{T}}(\mathbf{x}_0, \mathbf{x}_1, \mathbf{x}_2)). \end{aligned}$$

That is, as the composition

$$\eta_\Sigma = \eta \circ \tilde{\mathbf{T}} : \mathcal{T}_\Sigma \longrightarrow [1, \infty). \tag{8}$$

Note that η_Σ is a distortion measure on Σ since it is the composition of a planar distortion measure η, and a change of variable of the plane where t_Σ lies. Moreover, the reciprocal of η_Σ,

$$q_\Sigma := \frac{1}{\eta_\Sigma} : \mathcal{T}_\Sigma \longrightarrow [0, 1],$$

is also a quality measure, in the sense of [17]. It is important to point out that this quality measure holds the same properties of the corresponding original planar quality measure q.

Finally, we use the expression of the distortion η_Σ, Equation (8), to define the distortion and quality measures in terms of the parametric coordinates of the triangle.

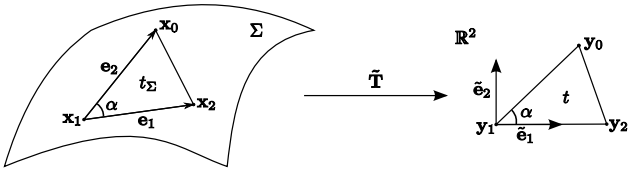

Fig. 2 Vector edges $\mathbf{e}_1$ and $\mathbf{e}_2$ for a triangle $t_\Sigma = (\mathbf{x}_0, \mathbf{x}_1, \mathbf{x}_2)$ on a surface Σ, and diagram of function $\tilde{\mathbf{T}}$.

Definition 1 The *distortion measure for triangles on parametric coordinates* is:

$$\eta_\mathcal{U} := \eta_\Sigma \circ \tilde{\varphi} = \eta \circ \tilde{\mathbf{T}} \circ \tilde{\varphi} : \mathcal{T}_\mathcal{U} \longrightarrow [1, \infty). \tag{9}$$

Definition 2 The *quality measure for triangles on parametric coordinates* is:

$$q_\mathcal{U} := \frac{1}{\eta_\mathcal{U}} : \mathcal{T}_\mathcal{U} \longrightarrow [0, 1]. \tag{10}$$

3.3 Properties of the proposed mappings

The following remarks highlight several properties of the mappings $\mathbf{T}$ and $\tilde{\mathbf{T}}$. Specifically, these properties help to: simplify the implementation, provide a geometrical interpretation of the mappings, and improve the numerical robustness of the method.

Remark 1 We derive a geometrical interpretation of mapping $\tilde{\mathbf{T}}$, Equation (7), in A.1. Specifically, we have that

$$\mathbf{T}(\mathbf{x}_1) = (0, 0)^T, \tag{11}$$

$$\mathbf{T}(\mathbf{x}_2) = (\|\mathbf{e}_1\|, 0)^T, \tag{12}$$

$$\mathbf{T}(\mathbf{x}_0) = (\|\mathbf{e}_2\| \ \cos(\alpha), \gamma\ \|\mathbf{e}_2\|\ |\sin(\alpha)|)^T, \tag{13}$$

where α the inner angle defined between $\mathbf{e}_1$ and $\mathbf{e}_2$ (see Figure 2).

Remark 2 From Equations (11) and (12), we realize that $\mathbf{T}(\mathbf{x}_1)$ and $\mathbf{T}(\mathbf{x}_2)$ are independent of the node $\mathbf{x}_0$. This is of the major importance when using the distortion measure to smooth a surface mesh, since it simplifies the final expression when smoothing in terms of the node $\mathbf{x}_0 = \varphi(\mathbf{u}_0)$.

Remark 3 By means of function $\tilde{\mathbf{T}}$, Equation (7), any element is always translated to the origin when its distortion measure is analyzed. This is of the major importance for the robustness of the optimization process. Specifically, the coordinates of the nodes of that element are then of similar magnitude, without regards to the physical location of the free node in the geometry.

3.4 Properties of the proposed measures

In this section, we first prove that the defined measure is independent of the surface parameterization.

Proposition 1 *Let $\varphi_1 : \mathcal{U}_1 \to \Sigma$ and $\varphi_2 : \mathcal{U}_2 \to \Sigma$ be two different diffeomorphic parameterizations of Σ. Let $\mathcal{M}$ be a mesh on Σ, and t_Σ a triangle with the vertices on the surface. Then, the distortion measure for triangles on parametric coordinates associated to t_Σ, see Equation (9), is independent of the surface parameterization.*

Proof Since both parameterizations are diffeomorphisms, we can write

$$t_\Sigma = (\mathbf{x}_1, \mathbf{x}_2, \mathbf{x}_3) = \tilde{\varphi}_1(\mathbf{u}_1^1, \mathbf{u}_2^1, \mathbf{u}_3^1) = \tilde{\varphi}_2(\mathbf{u}_1^2, \mathbf{u}_2^2, \mathbf{u}_3^2),$$

for unique $\mathbf{u}_j^i \in \mathcal{U}_i,\ i = 1, 2,\ j = 1, 2, 3$. Then,

$$\begin{aligned}\eta_{\mathcal{U}_1}(\mathbf{u}_1^1, \mathbf{u}_2^1, \mathbf{u}_3^1) &= \eta_\Sigma(\tilde{\varphi}_1(\mathbf{u}_1^1, \mathbf{u}_2^1, \mathbf{u}_3^1)) = \eta_\Sigma(\mathbf{x}_1, \mathbf{x}_2, \mathbf{x}_3) \\ &= \eta_\Sigma(\tilde{\varphi}_2(\mathbf{u}_1^2, \mathbf{u}_2^2, \mathbf{u}_3^2)) = \eta_{\mathcal{U}_2}(\mathbf{u}_1^2, \mathbf{u}_2^2, \mathbf{u}_3^2),\end{aligned}$$

where η_Σ is the distortion of the triangle with the vertices on the surface, see Equation (8). In fact,

$$\eta_{\mathcal{U}_1} = \eta_{\mathcal{U}_2} \circ (\tilde{\varphi}_2^{-1} \circ \tilde{\varphi}_1)$$

where $\tilde{\varphi}_2^{-1} \circ \tilde{\varphi}_1$ is a diffeomorphic change of variables, as stated in the Proposition entitled *Change of Parameters* in [3]. That is, functions $\eta_{\mathcal{U}_1}$ and $\eta_{\mathcal{U}_2}$ only differ by a change of variables.

Note that the distortion measure for triangles on parametric coordinates $\eta_\mathcal{U}$ (Definition 1) is a distortion measure, since: it is independent of the parameterization (Proposition 1), and it is defined in terms of the distortion measure η_Σ. Respectively, the quality measure for triangles on parametric coordinates, Definition 2, is a quality measure as stated in [17], that holds the same properties of the corresponding planar quality measure q.

Second, we also present a simplified expression for the distortion measure for triangles on parametric coordinates, see Equation (9), when there is one free node in the triangle and the rest of nodes are fixed.

Remark 4 Let $\mathbf{u}$ be the free node of a triangle and $\mathbf{u}_1$ and $\mathbf{u}_2$ the two fixed nodes. In A.2, we prove that for fixed values of $\mathbf{u}_1$ and $\mathbf{u}_2$, the restriction of $\eta_\mathcal{U}$ to a free node $\mathbf{u}$, $\eta_\mathcal{U}(\mathbf{u}; \mathbf{u}_1, \mathbf{u}_2)$, corresponds to the expression

$$\begin{array}{ccccccc}\hat{\eta}_\mathcal{U} : \mathcal{U} \subset \mathbb{R}^2 & \xrightarrow{\varphi} & \Sigma \subset \mathbb{R}^3 & \xrightarrow{\mathbf{T}} & \mathbb{R}^2 & \xrightarrow{\hat{\eta}} & \mathbb{R} \\ \mathbf{u} & \longmapsto & \varphi(\mathbf{u}) & \longmapsto & \mathbf{T}(\varphi(\mathbf{u})) & \longmapsto & \hat{\eta}(\mathbf{T}(\varphi(\mathbf{u}))),\end{array}$$

where

$$\hat{\eta}(\mathbf{y}) := \eta(\mathbf{y}, \mathbf{y}_1, \mathbf{y}_2), \tag{14}$$

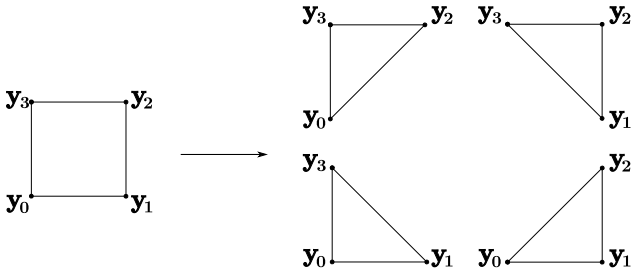

Fig. 3 Decomposition of a planar quadrilateral into four triangles.

$\mathbf{y}_1 := (0\ 0)^T$ (Equation (11)), and $\mathbf{y}_2 := (\|\mathbf{e}_1\|\ 0)^T$ (Equation (12)). That is, it corresponds to the composition

$$\hat{\eta}_\mathcal{U} = \hat{\eta} \circ \mathbf{T} \circ \varphi : \mathcal{U} \subset \mathbb{R}^2 \longrightarrow [1, \infty), \tag{15}$$

referred as the *restricted distortion measure for triangles on parametric coordinates*.

3.5 Extension to quadrilaterals on parametric coordinates

According to [19], the distortion measure for a planar quadrilateral is evaluated through the decomposition of the quadrilateral into four triangles, see Figure 3. In this work, we also compute the distortion measure of a quadrilateral element on a parameterized surface as the mean value of the distortion measure of the four corner triangles. To this end, let $(\mathbf{x}_0, \mathbf{x}_1, \mathbf{x}_2, \mathbf{x}_3)$ be the vertices of a quadrilateral element of a mesh with the nodes on a parameterized surface, and let $(\mathbf{u}_0, \mathbf{u}_1, \mathbf{u}_2, \mathbf{u}_3)$ be their parametric coordinates.

Definition 3 The *distortion measure for quadrilaterals on parametric coordinates* is:

$$\begin{aligned}\eta_\mathcal{U}(\mathbf{u}_0, \mathbf{u}_1, \mathbf{u}_2, \mathbf{u}_3) := \frac{1}{4}(&\eta_\mathcal{U}(\mathbf{u}_0, \mathbf{u}_1, \mathbf{u}_2) + \eta_\mathcal{U}(\mathbf{u}_0, \mathbf{u}_1, \mathbf{u}_3) + \\ &\eta_\mathcal{U}(\mathbf{u}_0, \mathbf{u}_2, \mathbf{u}_3) + \eta_\mathcal{U}(\mathbf{u}_1, \mathbf{u}_2, \mathbf{u}_3)),\end{aligned}$$

where $\eta_\mathcal{U}(\mathbf{u}_i, \mathbf{u}_j, \mathbf{u}_k)$ is the distortion on parametric coordinates for the triangle $(\mathbf{u}_i, \mathbf{u}_j, \mathbf{u}_k) \in \mathcal{T}_\mathcal{U}$, see Definition 1.

Definition 4 The *quality measure for quadrilaterals on parametric coordinates* is:

$$q_\mathcal{U}(\mathbf{u}_0, \mathbf{u}_1, \mathbf{u}_2, \mathbf{u}_3) := \frac{1}{\eta_\mathcal{U}(\mathbf{u}_0, \mathbf{u}_1, \mathbf{u}_2, \mathbf{u}_3)}. \tag{16}$$

Note that it is straightforward to prove that $q_\mathcal{U}$, Definition 4, verifies the properties a quality measure should hold according to [17]. In addition, we also present

a simplified expression for the distortion measure for quadrilaterals on parametric coordinates when there is one free node in the quadrilateral and the rest of nodes are fixed. The main purpose of this expression is to simplify the implementation of the optimization procedure.

Remark 5 Let $\mathbf{u}$ be the free node of a quadrilateral and $\mathbf{u}_1$, $\mathbf{u}_2$ and $\mathbf{u}_3$ the fixed nodes. We define the *restricted distortion measure for quadrilaterals on parametric coordinates* as

$$\hat{\eta}_{\mathcal{U}}(\mathbf{u}) := \frac{\hat{\eta}^1_{\mathcal{U}}(\mathbf{u}) + \hat{\eta}^2_{\mathcal{U}}(\mathbf{u}) + \hat{\eta}^3_{\mathcal{U}}(\mathbf{u}) + \eta_{\mathcal{U}}(\mathbf{u}_1, \mathbf{u}_2, \mathbf{u}_3)}{4}, \tag{17}$$

where $\hat{\eta}^i_{\mathcal{U}}(\mathbf{u})$ for $i = 1, 2, 3$ is the restricted distortion measure for the ith subtriangle, see Equation (15), and $\eta_{\mathcal{U}}(\mathbf{u}_1, \mathbf{u}_2, \mathbf{u}_3)$ is a constant term, see Equation (9). It is important to point out that this extension for quadrilateral elements require that the surface does not present self-intersections. Note that this is true if the surface parameterization is smooth and globally invertible, as we assumed in Section 3.1.

4 Optimization of surface mesh quality

In this section, we present an algorithm to optimize the distortion (quality) measure of triangular and quadrilateral meshes on parameterized surfaces. First, we formulate the optimization problem. Second, we present the proposed implementation. Third, we describe the proposed algorithm. Finally, we specify some implementation details.

4.1 Global formulation: imposing an ideal mesh distortion in the least-squares sense

The main goal of a simultaneous smoothing and untangling method is to obtain high-quality meshes composed by valid (non-inverted) elements. Note that the best possible result, can be characterized in terms of the distortion measure. That is, given a distortion measure $\eta_{\mathcal{U}}$ and a mesh $\mathcal{M}$ on a parameterized surface composed by n_N nodes and n_E elements, the node location is ideal if

$$\eta_{\mathcal{U}}(t^j_{\mathcal{U}}) = 1 \qquad j = 1, \dots, n_E, \tag{18}$$

where $t^j_{\mathcal{U}} = (\mathbf{u}_{j_1}, \dots, \mathbf{u}_{j_s})$ is the jth element expressed on parametric coordinates ($s = 3$ for triangles, $s = 4$ for quadrilaterals). However, for a fixed mesh topology the node location that leads to an ideal mesh distortion is not in general achievable. That is, the constraints in Equation (18) cannot be imposed strongly and therefore, we just enforce the ideal mesh distortion in the least-squares sense.

For a given mesh topology and a set of fixed nodes (nodes on the surface boundary), we formulate the least-squares problem in terms of the parametric coordinates of a set of free nodes (inner nodes on the surface). To this end, we reorder the parametric coordinates of the nodes, $\mathbf{u}_i$, in such a way that $i = 1, \dots, n_F$ are the indices corresponding to the free nodes, and $i = n_F + 1, \dots, n_N$ correspond to the fixed nodes. Thus, we can formulate the mesh optimization problem as

$$\begin{aligned} &\min_{\mathbf{u}_1,\dots,\mathbf{u}_{n_F}} f(\mathbf{u}_1, \dots, \mathbf{u}_{n_F}; \mathbf{u}_{n_F+1}, \dots, \mathbf{u}_{n_N}) = \\ &\min_{\mathbf{u}_1,\dots,\mathbf{u}_{n_F}} \tfrac{1}{2} \textstyle\sum_{j=1}^{n_E} (\eta_{\mathcal{U}}(t^j_{\mathcal{U}}) - 1)^2, \end{aligned} \tag{19}$$

where

$$f(\mathbf{u}_1, \dots, \mathbf{u}_{n_F}; \mathbf{u}_{n_F+1}, \dots, \mathbf{u}_{n_N}) := \frac{1}{2} \sum_{j=1}^{n_E} (\eta_{\mathcal{U}}(t^j_{\mathcal{U}}) - 1)^2$$

denotes the objective function.

Finally, the optimal configuration is found between the candidates for the minimization of (19). The candidates are the critical parametric coordinates $(\mathbf{u}_1, \dots, \mathbf{u}_{n_F})$ of f. They are characterized by

$$\begin{aligned} &\tfrac{\partial f}{\partial \mathbf{u}_i}(\mathbf{u}_1, \dots, \mathbf{u}_{n_F}; \mathbf{u}_{n_F+1}, \dots, \mathbf{u}_{n_N}) = \\ &\textstyle\sum_{j=1}^{n_E} (\eta_{\mathcal{U}}(t^j_{\mathcal{U}}) - 1) \ \tfrac{\partial \eta_{\mathcal{U}}}{\partial \mathbf{u}_i}(t^j_{\mathcal{U}}) = 0, \ i = 1, \dots, n_F. \end{aligned} \tag{20}$$

Notice that these conditions are expressed in terms of $\eta_{\mathcal{U}}$, which is independent of the surface parameterization. Therefore, we can proof the following result.

Proposition 2 *According to the objective function f, the optimal location for the mesh nodes $\mathbf{x}_i = \varphi(\mathbf{u}_i) \in \Sigma$, $i = 1, \dots, n_F$, is independent of the surface parameterization.*

Proof The conditions for the critical points of f are expressed in terms of $\eta_{\mathcal{U}}$ and its derivatives, Equation (20). Since $\eta_{\mathcal{U}}$ is independent of the surface parameterization, Proposition 1, the critical points of f are also independent of the surface mesh parameterization. To finalize, the optimal configurations are also independent of the surface parameterization since they are found between the candidate configurations.

Remark 6 In Proposition 2, we have proved that the candidate configurations are independent of the surface parameterization. In particular, the candidate configurations have to be the same for high (smooth Jacobian) and low quality (highly varying Jacobian) surface parameterizations. Therefore, the proposed method can be applied to obtain candidate mesh configurations on CAD surfaces represented by low-quality parameterizations.

Remark 7 The goal of the proposed method is to obtain the critical points independently of the surface parameterization. However, there are meshes that cannot be untangled by the proposed method, such as when the boundary edges of the mesh present self-intersections. Nevertheless, the proposed method has properly smoothed and untangled all the tested meshes.

4.2 Local implementation: deviation of the submesh distortion with respect to an ideal configuration

To solve the optimization problem in Equation (19), we have to find the optimum between the candidate configurations. These configurations are characterized by the global non-linear constraints in Equation (20). These global constraints can be solved by means of a local [12] or a global [23,22] non-linear solver. In our implementation, we choose a local non-linear iterative method that: exploits the locality of the problem, avoids solving large linear systems, and is well suited for parallelization (by coloring the mesh nodes). Specifically, we use a non-linear iterative Gauss-Seidel method determined by the iteration for $i = 1, \dots, n_F$

$$\mathbf{u}_i^{k+1} = \mathbf{u}_i^k - \alpha_i^k \; [\boldsymbol{\nabla}_{ii}^2 f(\mathbf{w}_i^k)]^{-1} \; \boldsymbol{\nabla}_i f(\mathbf{w}_i^k) \tag{21}$$

where α_i^k is the step length, and

$$\mathbf{w}_i^k = (\mathbf{u}_1^{k+1}, \dots, \mathbf{u}_{i-1}^{k+1}, \mathbf{u}_i^k, \mathbf{u}_{i+1}^k, \dots, \mathbf{u}_{n_F}^k; \mathbf{u}_{n_F+1}^0, \dots, \mathbf{u}_{n_N}^0)$$

is the vector of updated node locations for the $i-1$ first nodes. Note that $\boldsymbol{\nabla}_i$ and $\boldsymbol{\nabla}_{ii}^2$ denote the gradient and the Hessian with respect to the parametric coordinates $\mathbf{u}_i$ of node i.

To implement this iterative non-linear solver, we have to compute the gradient $\boldsymbol{\nabla}_i f$, the Hessian $\boldsymbol{\nabla}_{ii}^2 f$, and the step length, α_i^k. We first observe that the computation of the gradient

$$\boldsymbol{\nabla}_i f = \sum_{j=1}^{n_E} (\eta_{\mathcal{U}}(t_{\mathcal{U}}^j) - 1) \; \frac{\partial \eta_{\mathcal{U}}}{\partial \mathbf{u}_i}(t_{\mathcal{U}}^j),$$

can be simplified. That is, the distortion $\eta_{\mathcal{U}}(t_{\mathcal{U}}^j)$ only depends on the coordinates of the nodes of the element $t_{\mathcal{U}}^j$. Therefore, we have that

$$\frac{\partial \eta_{\mathcal{U}}}{\partial \mathbf{u}_i}(t_{\mathcal{U}}^j) = 0$$

for all the elements j that do not contain the node i. Thus, the gradient can be evaluated as

$$\boldsymbol{\nabla}_i f = \sum_{j \sim i} (\eta_{\mathcal{U}}(t_{\mathcal{U}}^j) - 1) \; \frac{\partial \eta_{\mathcal{U}}}{\partial \mathbf{u}_i}(t_{\mathcal{U}}^j),$$

where $j \sim i$ denotes that the summation is performed only for the elements that contain the node i. Now, taking into account the definition of the restricted distortion measure, see Equation (15) for triangles and Equation (17) for quadrilaterals, we have that

$$\boldsymbol{\nabla}_i f = \sum_{j \sim i} (\hat{\eta}_{\mathcal{U}}(\mathbf{u}_i) - 1) \; \frac{\partial \hat{\eta}_{\mathcal{U}}}{\partial \mathbf{u}_i}(\mathbf{u}_i).$$

Therefore, if we define

$$\hat{f}(\mathbf{u}_i) := \sum_{j \sim i} \left(\hat{\eta}_{\mathcal{U}}^j(\mathbf{u}_i) - 1\right)^2, \tag{22}$$

we have that

$$\boldsymbol{\nabla}_i f(\mathbf{u}_1, \dots, \mathbf{u}_{n_F}; \mathbf{u}_{n_F+1}, \dots, \mathbf{u}_{n_N}) = \boldsymbol{\nabla}_i \hat{f}(\mathbf{u}_i) \tag{23}$$

Moreover, the Hessian can be computed as

$$\boldsymbol{\nabla}_{ii}^2 f(\mathbf{u}_1, \dots, \mathbf{u}_{n_F}; \mathbf{u}_{n_F+1}, \dots, \mathbf{u}_{n_N}) = \boldsymbol{\nabla}_{ii}^2 \hat{f}(\mathbf{u}_i) \tag{24}$$

Finally, we have to compute the step length α_i^k. To this end, we use the Backtracking Line Search algorithm [25] detailed in Algorithm 1, where we set: $\alpha = 1$, $\rho = 0.5$ and $c = 10^{-4}$. Note that in this algorithm, we have to evaluate the global objective function f and its gradient to check the sufficient decrease condition in Line 4. By Equation (23), the sufficient decrease condition is equivalent to

$$f(\mathbf{w}_i^\alpha) > f(\mathbf{w}_i^k) + c\alpha [\boldsymbol{\nabla}_i \hat{f}(\mathbf{u}_i^k)]^T \mathbf{p}_i^k,$$

where $\mathbf{w}_i^\alpha$ is defined in Line 3 of Algorithm 1. Moreover, we have that

$$f(\mathbf{w}_i^\alpha) - f(\mathbf{w}_i^k) = \hat{f}(\mathbf{u}_i^\alpha) - \hat{f}(\mathbf{u}_i^k),$$

since the contributions of the elements that do not depend on the free node are mutually cancelled, being $\mathbf{u}_i^\alpha = \mathbf{u}_i^k + \alpha \mathbf{p}_i^k$. Therefore, the sufficient decrease condition is equivalent to

$$\hat{f}(\mathbf{u}_i^\alpha) > \hat{f}(\mathbf{u}_i^k) + c\alpha [\boldsymbol{\nabla}_i \hat{f}(\mathbf{u}_i^k)]^T \mathbf{p}_i^k. \tag{25}$$

Taking into account Equations (23), (24), and (25), we conclude that in the implementation we only need to compute the gradients, the Hessian, and the value of the local function $\hat{f}$ introduced in Equation (22).

Algorithm 1 Backtracking Line Search

```
1: function BackLineSearch(Vector w_i^k, Vector p_i^k)
2:     Set α > 0, ρ ∈ (0,1), c ∈ (0,1);
3:     w_i^α ← w_i^k + (0,...,0, αp_i^k, 0,...,0);
4:     while f(w_i^α) > f(w_i^k) + cα[∇_i f(w_i^k)]^T p_i^k do
5:         α ← ρα;
6:         w_i^α ← w_i^k + (0,...,0, αp_i^k, 0,...,0);
7:     end while
8:     return α;
9: end function
```

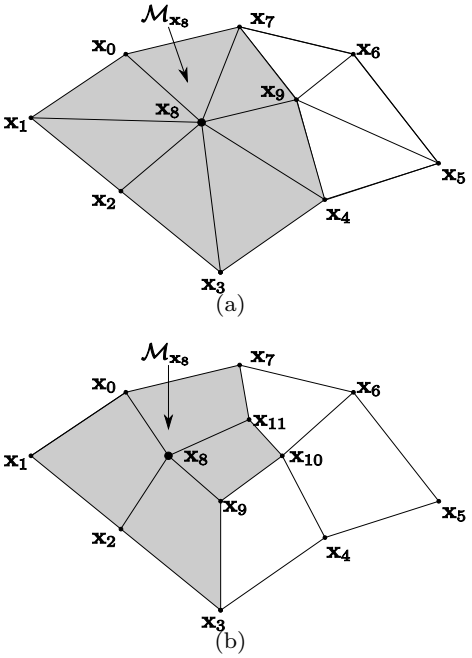

Fig. 4 Local submeshes in the physical space (marked in grey) of node $\mathbf{x}_8$ on a: (a) triangular surface mesh, and (b) quadrilateral surface mesh.

In our implementation, we exploit the computational reduction associated with the evaluation of the function $\hat{f}$. To this end, we denote by $\mathcal{M}_{\mathbf{u}}$ the elements that contain a free node $\mathbf{u}$. The set of elements $\mathcal{M}_{\mathbf{u}}$ is referred as the *submesh* associated with node $\mathbf{u}$. Figure 4 illustrates the submesh associated to a node for a triangular and a quadrilateral surface mesh. In the following remark, we use this notation to reinterpret the local function $\hat{f}$ as a measure of the deviation of the submesh distortion with respect to an ideal configuration. In addition, we state the optimized implementation for the non-linear iterative method.

Remark 8 Let $\mathbf{u}_i^k$ be the parametric coordinates of node i at step k, and let $\mathcal{M}_{\mathbf{u}_i^k}$ be the corresponding associated submesh composed by m_i elements. Let $\hat{\eta}_{\mathcal{U}}^j(\mathbf{u}_i)$ be the restricted distortion measure on the jth element of $\mathcal{M}_{\mathbf{u}_i^k}$, see Equation (15) for triangles and Equation (17) for quadrilaterals. We say that

$$\hat{f}(\mathbf{u}_i) = \sum_{j\sim i} \left(\hat{\eta}_{\mathcal{U}}^j(\mathbf{u}_i) - 1\right)^2 = \sum_{j=1}^{m_i} \left(\hat{\eta}_{\mathcal{U}}^j(\mathbf{u}_i) - 1\right)^2 \qquad (26)$$

is a local merit function that measures the *deviation with respect to an ideal configuration of the submesh distortion associated with* $\mathbf{u}_i$. According to this merit function, and to Equations (23), (24), and (25), we can implement the iteration $k+1$ for node i, $i = 1, \ldots, n_F$,

Algorithm 2 Optimization Algorithm

1: **function** SmoothMesh(Mesh $\mathcal{M}$)
2: $r_x,\ r_f \leftarrow \infty$; $tol_x \leftarrow 10^{-3}$; $tol_f \leftarrow 10^{-3}$; $k \leftarrow 0$;
3: $n_F \leftarrow$ number of free nodes of $\mathcal{M}$;
4: $f^0 \leftarrow f(\mathbf{w}_{n_F}^0)$;
5: **while** $r_x > tol_x$ or $r_f > tol_f$ **do**
6: $r_x,\ r_f \leftarrow 0$;
7: **for** $i = 1 : n_F$ **do**
8: $(\mathbf{u}_i^k, \mathbf{x}_i^k) \leftarrow$ coord. ith free node at kth step;
9: SetIdealElements(Submesh $\mathcal{M}_{\mathbf{u}_i^k}$);
10: $\mathbf{u}_i^0 \leftarrow$ SetInitialPoint(Submesh $\mathcal{M}_{\mathbf{u}_i^k}$);
11: $\mathbf{u}_i^{k+1} \leftarrow$ OptimizeSubmesh($\mathbf{u}_i^0$, Submesh $\mathcal{M}_{\mathbf{u}_i^0}$);
12: $\mathbf{x}_i^{k+1} \leftarrow \varphi(\mathbf{u}_i^{k+1})$;
13: $\mathcal{M} \leftarrow$ update $\mathbf{u}_i^{k+1}$ and $\mathbf{x}_i^{k+1}$ in $\mathcal{M}$;
14: $r_x^i \leftarrow \frac{\|\mathbf{x}_i^k - \mathbf{x}_i^{k+1}\|}{\text{max edge submesh } \mathcal{M}_{\mathbf{u}_i^k}}$;
15: $r_x \leftarrow \max(r_x, r_x^i)$;
16: **end for**
17: $f^{k+1} \leftarrow f(\mathbf{w}_{n_F}^{k+1})$;
18: $r_f \leftarrow \frac{\|f^k - f^{k+1}\|}{f^{k+1}}$;
19: $k \leftarrow k+1$;
20: **end while**
21: **return** Mesh $\mathcal{M}$;
22: **end function**

of the proposed non-linear method, Equation (21), as

$$\mathbf{u}_i^{k+1} = \mathbf{u}_i^k - \alpha_i^k \ [\boldsymbol{\nabla}_{ii}^2 \hat{f}(\mathbf{u}_i^k)]^{-1} \ \boldsymbol{\nabla}_i \hat{f}(\mathbf{u}_i^k). \qquad (27)$$

4.3 Optimization algorithm

In this section, we detail the implementation of the optimization procedure developed in Section 4.1. To this end, we consider Algorithm 2, where until convergence is achieved, Line 5, a loop on all the free nodes is performed, Line 7. Specifically, convergence is achieved when of the maximum of the relative displacement of the nodes between step k and step $k+1$ (Line 15) and the relative error of the objective function (Line 18) are both below a given tolerance. Then, for each free node three functions are called: SetIdealElements, SetInitialPoint and OptimizeSubmesh.

Function SetIdealElements, Line 9, determines the ideal for each element of the submesh associated with the current free node. The determination of the ideal element depends on the selected distortion measure. In this work, we only select measures that quantify the shape or the size of isotropic physical elements, see Section 4.4. For the shape measure, SetIdealElements sets the same ideal element (an equilateral triangle, or square) for all the elements of the mesh. Whereas, for the size measure, it sets the same ideal shape (an equilateral triangle, or square) with a variable size that depends on a prescribed element size field. The ideal

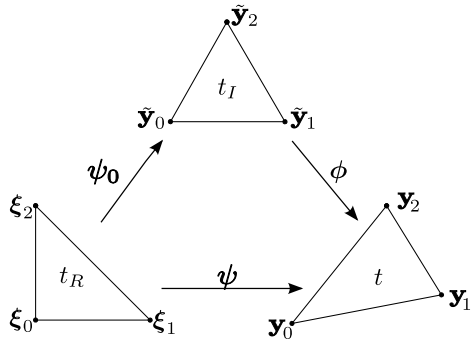

Fig. 5 Mappings between the reference, the ideal and the physical elements.

size is determined as the average of the size field evaluated on the nodes of the current element.

Next, SetInitialPoint sets the current location of the node as the initial guess for the minimization process, Line 10. If the initial guess is tangled, we use the untangling technique presented in [6], see details in Section 4.4 and B.

Finally, OptimizeSubmesh, Line 11, computes the update $k+1$ of node i determined by Equation (27). It is important to point out that, according to Remark 3, the elements of the submesh are translated to the origin, enhancing the robustness of the optimization process. In C, we deduce the analytical expressions of the first and second order derivatives of the objective function $\hat{f}(\mathbf{u})$. Recall that if it is not possible to compute second order derivatives of the surface parameterization, the presented approach is still applicable. Other methods (with lower convergence rates) such as the Steepest Descent can be used in order to determine the advancing direction in Equation (27).

4.4 Inclusion of several distortion measures

We apply the presented approach to define distortion and quality measures on parameterized surfaces to three Jacobian algebraic distortion measures for planar elements, presented in [17]. Specifically, we consider a shape, a size, and a size-shape measure. Moreover, we detail how to modify these measures to incorporate the untangling capability to the optimization method. To this end, we use the modification presented in [6]. This modification can be applied to distortion measures where the determinant of the Jacobian appears in the denominator.

In order to define a Jacobian-based measure for triangles, three types of elements are required: the reference, the ideal, and the physical. The reference element has an auxiliary use, since it is straight forward to define a linear affine mapping between the reference and any other triangle. The ideal triangle represents the best configuration of the geometrical property to quantify. The physical is the element to be measured. Once the mappings between the reference and the ideal and the physical elements are obtained, a mapping between the ideal and the physical elements is determined by (see Figure 5)

$$\boldsymbol{\phi} : t_I \xrightarrow{\boldsymbol{\psi}_0^{-1}} t_R \xrightarrow{\boldsymbol{\psi}} t.$$

The Jacobian of this affine mapping contains information about the deviation of the physical element with respect to the ideal. Hence, the distortion measure of the physical element is defined in terms of $\mathbf{S}(\mathbf{y}_0, \mathbf{y}_1, \mathbf{y}_2) = \mathbf{D}\boldsymbol{\phi}$. These distortion measures quantify the deviation of a geometrical property of the physical element with respect to the ideal element in a range scale $[1, \infty)$. Note that, in Section 3 we have defined the distortion and quality measures for quadrilateral element in terms of distortion and quality measures for triangles as in [19].

In this work, we consider three Jacobian distortion measures [17] where the determinant of the Jacobian appears in the denominator. To incorporate the untangling capability to the optimization method, $\sigma = \det(\mathbf{S})$ is replaced by

$$\sigma_\delta(\sigma) = \frac{1}{2}\left(\sigma + \sqrt{\sigma^2 + 4\delta^2}\right), \tag{28}$$

where δ is a numerical parameter that has to be determined [6]. Parameter δ is sensitive to the magnitude of σ. Thus, special attention has to be focused on its selection. In Appendix B, we derive a new formula to determine δ automatically, see Equation (38). This expression determines a δ parameter that slightly modifies the distortion measure to remove the appearance of vertical asymptotes. The parameter δ is only set to non-zero values when an invalid (tangled) configuration of the mesh is being optimized. Note that when $\delta > 0$ the distortion measure is a smooth function, see Appendix B, and therefore, its derivatives can be computed as detailed in Appendix C. For quality evaluation, or once all the elements are valid in the optimization process, δ is set to zero and therefore, the distortion measure is not modified.

Shape distortion measure

$$\eta_{sh}(\mathbf{y}_0, \mathbf{y}_1, \mathbf{y}_2) = \frac{\|\mathbf{S}(\mathbf{y}_0, \mathbf{y}_1, \mathbf{y}_2)\|^2}{2|\sigma_\delta(\mathbf{y}_0, \mathbf{y}_1, \mathbf{y}_2)|}, \tag{29}$$

where $\|\cdot\|$ is the Frobenius norm. This distortion measure quantifies the deviation of the shape of the physical triangle with respect to the ideal shape.

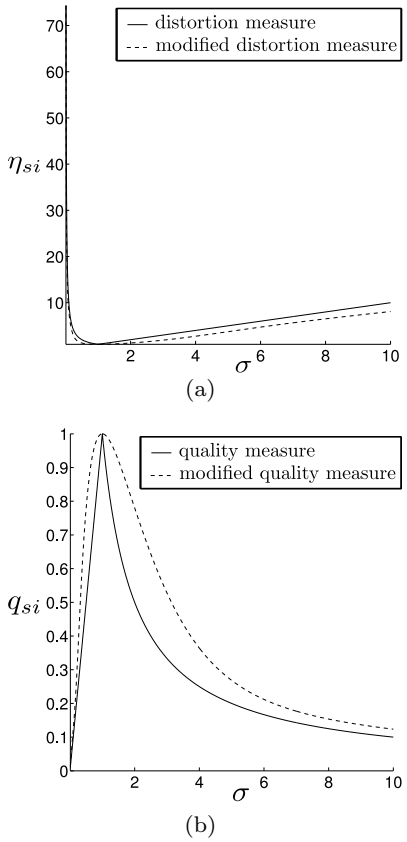

Fig. 6 Plots of the original and modified: (a) size distortion measure and (b) size quality measure.

Size distortion measure

$$\eta_{si}(\mathbf{y}_0, \mathbf{y}_1, \mathbf{y}_2) = \frac{1}{\mu(\sigma_\delta(\mathbf{y}_0, \mathbf{y}_1, \mathbf{y}_2))}, \tag{30}$$

where $\mu(\sigma) = \min(\sigma, \sigma^{-1})$. This distortion measure quantifies the deviation of the size of the element with respect to the size of the ideal triangle. The size of the ideal triangle is prescribed using a size field function, $h : \mathcal{U} \subset \mathbb{R}^2 \longrightarrow \mathbb{R}$, or using the size of the initial mesh. Note that in Equation (30), the term $\mu(\sigma)$ is not differentiable. Thus, it can not be used in a continuous optimization procedure. To overcome this drawback we propose to replace $\mu(\sigma)$ by a continuous and differentiable function that holds the same minimum and a similar behavior:

$$\mu_*(\sigma) = \frac{e}{2}\left(\sigma e^{-\sigma} + \sigma^{-1} e^{-\sigma^{-1}}\right). \tag{31}$$

Figure 6 plots the size distortion and the size quality measures using the original, $\mu(\sigma)$, and the modified functions, $\mu_*(\sigma)$, functions in terms of σ. It is worth to notice that using the modification presented in Equation (31), the size distortion measure, η_{si}, is still a distortion measure, i.e. it holds the properties stated in [17].

Size-shape distortion measure

$$\eta_{ss}(\mathbf{y}_0, \mathbf{y}_1, \mathbf{y}_2) = \eta_{sh}(\mathbf{y}_0, \mathbf{y}_1, \mathbf{y}_2)\ \eta_{si}(\mathbf{y}_0, \mathbf{y}_1, \mathbf{y}_2). \tag{32}$$

This distortion measure combines η_{sh} and η_{si}, see details in [17]. Thus, it quantifies both the size and the shape of the element.

4.5 Illustration of the smoothing and untangling procedure

To illustrate the proposed method, we consider an initially tangled quadrilateral mesh on a cylindrical surface. Specifically, we present the results obtained for the minimization of the shape distortion measure. Note that the position of the central node determines three invalid elements with zero shape quality (blue). Figure 7 presents the sequence of steps required to optimize an initially tangled configuration. We observe that the proposed optimization method ($\delta > 0$) requires just one step to relocate the central node and therefore, to untangle the mesh. To this end, the method also relocates the nodes surrounding the node that invalidates the mesh. Intuitively, the surrounding nodes help to accommodate the central node in a valid configuration. Once the mesh is untangled, the position of all the nodes is optimized ($\delta = 0$) to obtain a mesh composed by high-quality elements. In addition, in Figure 7(d) we show the final mesh and the different locations of the central node (white) during the optimization procedure.

5 Numerical examples

In this section, we present several examples in order to assess the properties of the proposed smoothing method: *1.* it is independent of the surface parameterization; *2.* it provides high-quality meshes even though the initial mesh contains a large number of tangled elements (robustness); *3.* it can incorporate several planar distortion measures in order to achieve different properties in the smoothed mesh, and *4.* it can be used to optimize surface meshes generated from industrial CAD models. For all the examples, we present a table summarizing the quality statistics of the meshes. Specifically, we provide: the minimum, the maximum, the mean and the standard deviation of the quality of the elements, and the number of tangled elements. We highlight that in all cases, the smoothed mesh increases the minimum and mean values of the mesh quality and decreases its standard deviation. All algorithms have been implemented in C++ in the meshing environment EZ4U [28,29,26].

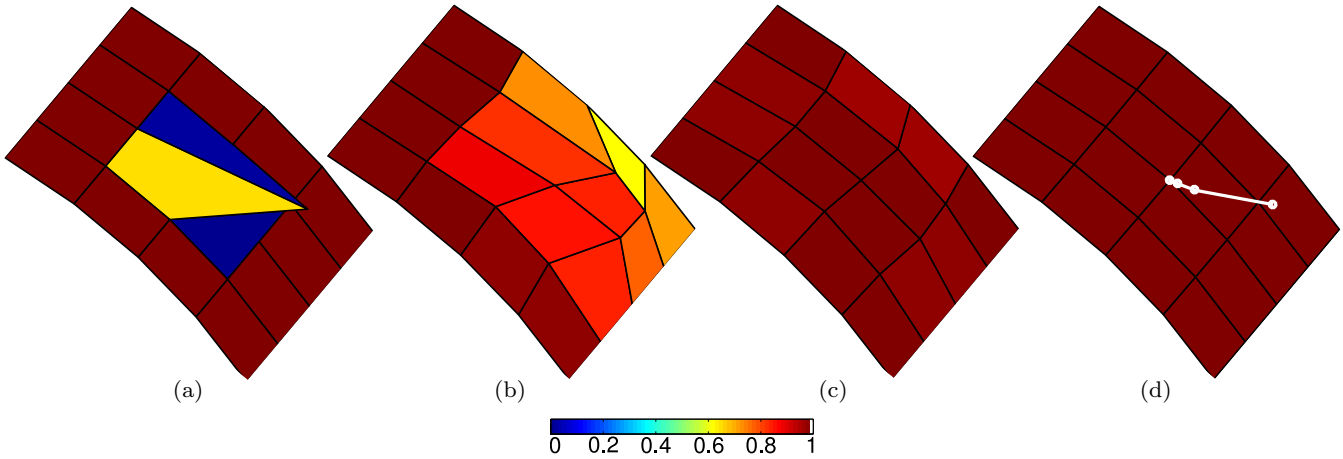

Fig. 7 Shape quality during the smoothing and untangling procedure for a quadrilateral mesh. Figures (a-d) present the four steps of the minimization procedure. Figure (d) presents in white the path of the central node.

5.1 Independence on the surface mesh parameterization

The aim of this example is to show that the proposed quality measure and the derived optimization procedure, are independent of the surface parameterization. To illustrate this property, we use the shape distortion measure, Equation (29), and we consider two surfaces, and for each one we define two different parameterizations. Moreover, we use a different type of element for each surface: triangles for the first one, and quadrilaterals for the second. For both surfaces, we show the meshes on the parametric space (first and third columns in Figure 8) and on the physical space (second and fourth columns in Figure 8). The meshes on the parametric space are colored according to the shape quality of the elements on the physical space.

Surface 1. Given the parameterization

$$\begin{aligned}\varphi_{\Sigma_1} : \mathcal{U}_{\Sigma_1} = [-1,1]^2 \subset \mathbb{R}^2 &\longrightarrow \mathbb{R}^3 \\ (u,v) &\longrightarrow (u,v,0),\end{aligned}$$

we define the surface $\Sigma_1 = \varphi_{\Sigma_1}(\mathcal{U}_{\Sigma_1})$. Note that this parameterization has a constant Jacobian. We define two different parameterizations for Σ_1:

$$\varphi^1_{\Sigma_1}(u,v) = (u, v\ \epsilon(u,v), 0), \text{ and}$$
$$\varphi^2_{\Sigma_1}(u,v) = (u\ \epsilon(u,v), v\ \epsilon(u,v), 0),$$

where $\epsilon(u,v) := e^{-2(1-u^2)(1-v^2)}$, with a non-constant Jacobian matrix.

For this case, the mesh is structured and composed by 722 triangular elements and 400 nodes. Note that the elements of the initial mesh on the parametric space are rectangular isosceles triangles (see Figures 8(a) and 8(e)). These meshes are mapped to the physical space according to $\varphi^1_{\Sigma_1}$ and $\varphi^2_{\Sigma_1}$ respectively, see Figures 8(b) and 8(f). Therefore, the initial meshes on the physical space follow approximately the isolines of the corresponding parameterization. Note that both meshes contain low-quality elements due to the use of parameterizations with varying Jacobian matrix. Figures 8(c) and 8(g) show the optimized meshes in the parametric domain, and Figures 8(d) and 8(h) show the optimized meshes on the surface. It is important to point out that the smoothing-untangling procedure, brought up with different parameterizations, obtains equal final meshes.

Surface 2. Given the parameterization

$$\begin{aligned}\varphi_{\Sigma_2} : \mathcal{U}_{\Sigma_2} = [-1,1]^2 \subset \mathbb{R}^2 &\longrightarrow \mathbb{R}^3 \\ (u,v) &\longrightarrow (u,v,\sin(\pi u)\cos(\pi u)).\end{aligned}$$

we define the surface $\Sigma_2 = \varphi_{\Sigma_2}(\mathcal{U}_{\Sigma_2})$. We define two different parameterizations for Σ_2:

$$\varphi^1_{\Sigma_2}(u,v) = (u, v\ \epsilon(u,v), \sin(\pi u)\ \cos(\pi v\ \epsilon(u,v)))\,, \text{ and}$$
$$\varphi^2_{\Sigma_2}(u,v) = (u\ \epsilon(u,v), v\ \epsilon(u,v), \sin(\pi u\ \epsilon(u,v))\ \cos(\pi v\ \epsilon(u,v))).$$

For this case, the mesh is structured and composed by 576 quadrilateral elements and 625 nodes. Note that the elements of the initial mesh on the parametric space are structured and square-shaped quadrilaterals, see Figures 8(i) and 8(m). The image of these meshes on the surface is presented in Figures 8(j) and 8(n). Again, the parameterizations lead to low quality meshes. The optimized meshes on the parametric surface are shown in Figures 8(k) and 8(o), and on the physical surface in Figures 8(l) and 8(p). Although in this case we have a non-planar surface, the smoothing-untangling procedure also provides the same meshes.

Table 1 presents the quality statistics for both surface meshes. Note that since we have used poor parameterizations the initial meshes have low quality. How-

ever, the optimization procedure can smooth the initial meshes and obtain a high-quality mesh (in both cases the minimum value of the quality is significantly increased). In addition, the smoothing-untangling procedure provides the same smoothed meshes up to minimization tolerance for any diffeomorphic parameterization.

5.2 Robustness of the smoothing and untangling procedure

In this section, we check the robustness of the developed smoothing and untangling method. To this end, we consider two different test cases. In the first case, we show that the proposed approach can untangle meshes composed by a large number of tangled elements. In the second case, we illustrate that this method can smooth and untangle meshes that present non-convex features on the boundary.

Dealing with a large number of tangled elements
In this test case, we use the shape distortion measure, Equation (29), and we consider two NURBS surfaces. The first one is meshed using triangular elements, and the second one is meshed with quadrilateral elements (see Figure 9). For each surface, three figures are presented. First, we display an initial mesh generated on the NURBS surface. Second, we show a mesh with the same topology than the initial one, but with a large number of tangled elements. This tangled mesh is the input of the smoothing and untangling algorithm. Third, we present the optimized mesh.

Figure 9(a) presents a triangular mesh generated on a revolution surface. This mesh is composed by 1200 nodes and 2242 elements. Figure 9(b) shows a mesh with 279 tangled elements, obtained by a random perturbation of the initial mesh. Figure 9(c) presents the optimized mesh obtained using the proposed method. Analogously, Figures 9(d), 9(e) and 9(f), present the same scheme for a quadrilateral mesh on a rolled surface. The mesh is composed by 3125 nodes and 2976 elements, and the perturbed configuration has 1589 tangled elements.

Table 2 summarizes the shape quality statistics of the meshes presented in Figure 9. Note that the proposed algorithm untangles an input mesh composed by a large number of tangled elements. In addition, for both cases, the proposed method improves the quality of the initial surface meshes.

Dealing with non-convex boundaries
In this test case, we show that the presented procedure is capable of smoothing and untangling meshes on domains with non-convex boundaries. To this end, we first generate a valid triangular mesh on a cylindrical surface with a non-convex boundary. Then, we compare the results obtained with a Laplacian smoother [15] with the proposed approach, Figure 10. First, we observe that, as expected, the Laplacian smoother obtains a final invalid configuration where four inverted elements appear close to the non-convex boundary of the domain. Second, we apply the proposed optimization procedure to the invalid mesh obtained with the Laplacian smoothing. The proposed procedure is able to obtain a mesh composed by valid elements and with a minimum shape quality of 0.22. Table 3 presents the shape quality statistics for both smoothing approaches. It is important to point out that for non-convex domains, the Laplacian smoother can tangle initially valid configurations. On the contrary, the proposed approach is able to untangle initially non-valid configurations for meshes on non-convex domains.

5.3 Preservation of an element size field

This example has two objectives. On the one hand, we emphasize that the proposed quality measure for meshes on parameterized surfaces can handle any quality for planar elements. On the other hand, we use this property to illustrate the capability of the proposed optimization procedure to maintain the prescribed element size while improving the shape of the elements. To this end, we generate a mesh on a cylindrical surface parameterized by

$$\begin{aligned}\varphi_{\Sigma} : \mathcal{U}_{\Sigma} = [-2,2]^2 \subset \mathbb{R}^2 &\longrightarrow \mathbb{R}^3 \\ (u,v) &\longrightarrow (\sin(\tfrac{\pi}{6}u), \cos(\tfrac{\pi}{6}v), \tfrac{\pi}{6}u),\end{aligned}$$

with the prescribed element size on the parametric space:

$$\begin{aligned}h : \mathcal{U}_{\Sigma} \subset \mathbb{R}^2 &\longrightarrow \mathbb{R} \\ (u,v) &\longrightarrow 0.2(\min(|u|,|v|) + 0.1).\end{aligned} \tag{33}$$

Note that $h(u,v)$ assigns size 0.02 on the axis of the parametric space and 0.42 at the corners, see Figure 11. First, we generate a triangular, Figure 12, and a quadrilateral mesh, Figure 13, on the cylindrical surface according to the element size field, Equation (33). Second, we optimize these meshes using: the shape (Equation (29)), the size (Equation (30)) and the size-shape (Equation (32)) distortion measures. Figures 12 and 13 show the obtained results, coloring the meshes according to the size-shape quality measure. Table 4 presents the shape quality statistics of the four meshes.

Figure 12(a) and 13(a) show the initial meshes. Figure 12(b) and 13(b) present the smoothed meshes using the shape distortion measure. Despite improving the

Srf.	Mesh	Fig.	Min.Q.	Max.Q.	Mean Q.	Std.Dev.	Tang.
$\varphi^1_{\Sigma_1}$	Initial	8(b)	0.23	0.99	0.61	0.20	0
	Smoothed	8(d)	0.87	0.87	0.87	0.00	0
$\varphi^1_{\Sigma_2}$	Initial	8(f)	0.28	1.00	0.60	0.20	0
	Smoothed	8(h)	0.87	0.87	0.87	0.00	0
$\varphi^2_{\Sigma_1}$	Initial	8(j)	0.15	1.00	0.60	0.24	0
	Smoothed	8(l)	0.88	1.00	0.97	0.03	0
$\varphi^2_{\Sigma_2}$	Initial	8(n)	0.34	0.99	0.64	0.17	0
	Smoothed	8(p)	0.88	1.00	0.97	0.03	0

Table 1 Shape quality statistics of the meshes on Σ_1 and Σ_2.

Srf.	Mesh	Fig.	Min.Q.	Max.Q.	Mean Q.	Std.Dev.	Tang.
Revol.	Initial	9(a)	0.63	0.90	0.79	0.07	0
	Tangled	9(b)	0.00	1.00	0.60	0.31	274
	Smoothed	9(c)	0.69	0.98	0.82	0.03	0
Rolled	Initial	9(d)	0.47	1.00	0.90	0.13	0
	Tangled	9(e)	0.00	0.98	0.22	0.27	1578
	Smoothed	9(f)	0.56	1.00	0.90	0.11	0

Table 2 Shape quality statistics of the meshes on the revolution and rolled surfaces.

Smoothing method	Fig.	Min.Q.	Max.Q.	Mean Q.	Std.Dev.	Tang.
Laplacian	10(a)	0.00	1.00	0.76	0.29	61
Proposed	10(b)	0.22	0.99	0.73	0.15	0

Table 3 Shape quality statistics for the optimized meshes on the cylinder.

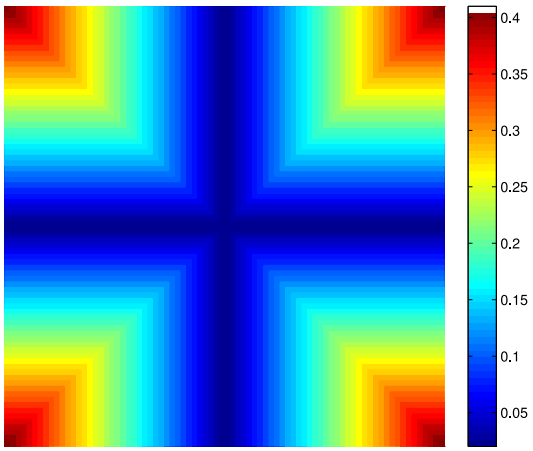

Fig. 11 Contour plot of the size field for the cylinder example.

shape of the elements, we observe that some spurious changes on the element size appear. Since this measure is scale-independent, it is free to change the prescribed size of the initial mesh to improve the shape. Figures 12(c) and 13(c) displays the smoothed meshes using the size distortion measure. Since this measure only involves the determinant of the Jacobian matrix (i.e. the area of the element multiplied by a constant), it optimizes the size of the elements according to the prescribed size field, but it is free to change the shape of the elements. Thus, it can be used to check if a given mesh verifies a prescribed size field, but distorted elements can appear on the final mesh if it is used in an optimization procedure. Figures 12(d) and 13(d) show the smoothed meshes using the size-shape distortion measure. Note that it improves the shape of the elements, and it also maintains the prescribed element size (no spurious changes of the element size appear). In practical applications, the element size field is defined in the physical space using, for instance, a background mesh. If that is the case, the optimization procedure using the size-shape function can also be used.

5.4 Surfaces composed of multiple patches

In this example, we apply the smoothing and untangling procedure using the shape distortion measure, Equation (29), to two CAD models composed by multiple patches: a linking rod and a propeller. Figure 14(a) shows the initial mesh on the linking rod. It is composed by 6386 nodes and 6388 quadrilateral elements. To illustrate the capabilities of the proposed method, the initial mesh has been generated without using any smoothing procedure. Thus, it contains degenerated elements. Figure 14(b) presents the smoothed mesh. Figure 15(a) presents the initial mesh on the propeller. It is composed by 4664 nodes and 9328 triangular elements. Figure 15(b) presents the resulting mesh from the smoothing procedure.

Table 5 details the shape quality statistics of the presented meshes. Note that the smoothing procedure properly improves the quality of the surface mesh in

Optimization Measure	Fig.	Min.Q.	Max.Q.	Mean Q.	Std.Dev.	Tang.
Not optimized	12(a)	0.41	1.00	0.87	0.11	0
Shape	12(b)	0.32	1.00	0.87	0.10	0
Size	12(c)	0.15	1.00	0.76	0.16	0
Size-shape	12(d)	0.53	1.00	0.89	0.07	0
Not optimized	13(a)	0.13	0.95	0.69	0.17	0
Shape	13(b)	0.15	0.95	0.68	0.16	0
Size	13(c)	0.09	0.89	0.48	0.17	0
Size-shape	13(d)	0.33	0.95	0.69	0.10	0

Table 4 Size-shape quality statistics for the triangular and quadrilateral meshes on the cylinder.

Surf.	Mesh	Fig.	Min.Q.	Max.Q.	Mean Q.	Std.Dev.	Tang.
Link.Rod	Initial	14(a)	0.00	1.00	0.91	0.20	231
	Smoothed	14(b)	0.29	1.00	0.94	0.08	0
Propeller	Initial	15(a)	0.24	1.00	0.93	0.08	0
	Smoothed	15(b)	0.64	1.00	0.94	0.05	0

Table 5 Shape quality statistics of the meshes on the linking rod and the propeller.

both cases. In addition, it increases the minimum and the mean value of the quality of the mesh.

5.5 Extension to high-order meshes

In this example, we outline and illustrate how the presented framework for smoothing and untangling linear triangular meshes on parameterized CAD surfaces can be extended to high-order meshes. To optimize high-order meshes, we propose to use the definition of quality measure for planar high-order triangles introduced in [27]. In that work, the distortion measure of a high-order planar triangle is defined as an integral on the triangle of a Jacobian distortion measure. That is, this distortion measure is computed in terms of the Jacobian of the high-order isoparametric mapping. Therefore, and similarly to our approach for linear elements, we can use any of the distortion measures detailed in Section 4.4. Note that the Jacobian of the surface element is a 3×2 non-constant matrix. Nevertheless, similarly to the approach detailed in Section 3.2 for linear elements, we can use the embedding (6) to extend the measures for planar high-order elements to elements on parameterized surfaces. Then, we consider to use a generalization of the process presented in Section 4.3 to optimize the high-order mesh on the CAD geometry.

To illustrate this generalization, we consider the CAD model of the propeller presented in Figure 15. First, we generate a low-quality mesh of interpolation degree five composed by 1374 elements and 18343 nodes that contains 153 tangled elements, see Figure 16(a). Then, we apply the extension of the method to high-order elements and obtain a high-quality mesh of interpolation degree five without any tangled element, see Figure 16(b). To highlight the improvement on the quality of the mesh, Figures 16(c) and 16(d) show a detail of the initial and optimized meshes, respectively. Table 6 displays the shape quality statistics of the initial and optimized meshes. Note that the procedure proposed for high-order meshes also simultaneously smoothes and untangles the mesh, removing inverted elements and improving the minimum and the overall quality of the high-order elements.

It is important to point out that detecting in a visual manner non-valid high-order elements is harder than with linear elements. In the linear case, there are two configurations of the element nodes that characterize a non-valid element. That is, the nodes are either clock-wise oriented or they determine a degenerated element (area 0). In the high-order case, an element is non-valid if the determinant of the Jacobian of the isoparametric mapping presents non-positive values. Several of the non-valid configurations can be identified visually such as when: the whole element is inverted; the element is degenerated (area 0); or the edges cross each other. However, there are configurations that can not be identified visually since the non-positive values of the determinant of the Jacobian appear in the interior of the element. That is, non-valid configurations can appear even when the interpolation nodes seem to be properly distributed. This is actually the explanation for the appearance of several of the non-valid elements in the initial mesh, colored in blue in Figures 16(a) and 16(c).

6 Concluding remarks

This paper presents two main contributions. First, we detail a new technique to extend any distortion (quality) measure defined for planar elements to parameterized surfaces. Similar to the planar case, it has been

Surf.	Mesh	Fig.	Min.Q.	Max.Q.	Mean Q.	Std.Dev.	Tang.
Propeller	Initial	16(a)	0.00	1.00	0.80	0.30	153
	Smoothed	16(b)	0.73	1.00	0.95	0.05	0

Table 6 Shape quality statistics for the meshes of interpolation degree five on the propeller.

developed for triangle elements and extended to quadrilateral elements. It is worth noticing that the proposed measure expresses the quality of the elements on the surface in terms of the parametric coordinates of its nodes. Second, we develop a continuous optimization procedure to improve (smooth and untangle) the quality of meshes on parameterized surfaces. Since the distortion (quality) measure is defined in terms of the parametric coordinates, the optimization procedure is also written in terms of the parametric coordinates. Thus, by construction, it ensures that the nodes are always placed on the surface, avoiding any additional constraint (*e.g.,* a projection procedure). It is important to point out that both, the measure (quality) definition and the optimization procedure, are independent of the surface parameterization. Therefore, this technique is particularly suited for smoothing meshes on multi-patch CAD surfaces defined by low-quality parameterizations.

To illustrate the capabilities of the proposed technique, we have selected three Jacobian-based distortion measures. The shape distortion measure optimizes the mesh focusing on the shape of the element. Thus, after the optimization process, some elements may not verify the prescribed element size. The size distortion measure improves the mesh taking into account the prescribed element size. Hence, poor-shaped elements can appear in the mesh after the optimization process. To overcome these drawbacks, we have also used the size-shape distortion measure that combines the previous distortion measures to produce a mesh that preserves a prescribed element size field and generates well-shaped elements. For these measures, we have detailed how to incorporate them in a continuous optimization procedure that allows untangling meshes. To quantify the advantages and disadvantages of the proposed approach, we have considered to perform in the near future an exhaustive comparison with other existing methods.

Finally, to underline the feasibility to extend this technique to high-order meshes on CAD surfaces, we have included a preliminary result of the optimization for a mesh of interpolation degree five on a propeller. However, further research is required in order to analyze several key issues of this extension. For instance, its independence of the quality of the parameterization, or its robustness to untangle high-order meshes. We have also considered to extend the proposed technique to smooth and untangle high-order tetrahedral and hexahedral meshes for domains with curved boundaries. To this end, we have planned a hierarchical and *a posteriori* approach: first, to generate a linear volume mesh; second, to curve the boundary faces; third, to smooth and untangle the boundary faces with the technique proposed in this work; and fourth, to smooth and untangle the elements in the interior of the volume mesh.

Acknowledgements

Partially supported by Spanish *Ministerio de Ciencia e Innovación* (DPI2011-23058) and by CUR from DIUE of the Generalitat de Catalunya and the European Social Fund (grants FI-DGR and BE-DGR).

A Further details

A.1 Derivation of Remark 1

In this appendix, we compute the image by mapping $\mathbf{T}$, Equation (6), of the three vertices of a triangle $t_\Sigma = (\mathbf{x}_0, \mathbf{x}_1, \mathbf{x}_2) \in \mathcal{T}_\Sigma$:

$$\mathbf{T}(\mathbf{x}_1) = \mathbf{M}\ (\mathbf{x}_1 - \mathbf{x}_1) = \begin{pmatrix} 0 \\ 0 \end{pmatrix},$$

$$\mathbf{T}(\mathbf{x}_2) = \mathbf{M}\ (\mathbf{x}_2 - \mathbf{x}_1) = \begin{pmatrix} \frac{\mathbf{e}_1^T}{\|\mathbf{e}_1\|} \\ \gamma\ (\tilde{\mathbf{e}}_{2,0})^T \end{pmatrix}\ \mathbf{e}_1 = \begin{pmatrix} \|\mathbf{e}_1\| \\ 0 \end{pmatrix},$$

$$\mathbf{T}(\mathbf{x}_0) = \mathbf{M}\ (\mathbf{x}_0 - \mathbf{x}_1) = \begin{pmatrix} \frac{\mathbf{e}_1^T \mathbf{e}_2}{\|\mathbf{e}_1\|} \\ \gamma\ \frac{\mathbf{e}_2^T \mathbf{e}_2 - (\mathbf{e}_2^T\ \tilde{\mathbf{e}}_1)\tilde{\mathbf{e}}_1^T \mathbf{e}_2}{\sqrt{\mathbf{e}_2^T \mathbf{e}_2 - (\mathbf{e}_2^T \tilde{\mathbf{e}}_1)^2}} \end{pmatrix}$$

$$= \begin{pmatrix} \|\mathbf{e}_2\| \cos(\alpha) \\ \gamma\ \sqrt{\|\mathbf{e}_2\|^2 - (\|\mathbf{e}_2\| \cos(\alpha))^2} \end{pmatrix}$$

$$= \begin{pmatrix} \|\mathbf{e}_2\|\ \cos(\alpha) \\ \gamma\ \|\mathbf{e}_2\|\ |\sin(\alpha)| \end{pmatrix}.$$

A.2 Derivation of the restricted distortion measure for a triangle on parametric coordinates

To restrict function $\eta_{\mathcal{U}}$, Equation (9), to function $\hat{\eta}_{\mathcal{U}}$, Equation (15), through the composition of φ, $\mathbf{T}$ and $\hat{\eta}$ (Equations (2), (6) and (14), respectively), we have to check that $\mathbf{y}_1$ and $\mathbf{y}_2$ in Equation (14) can be computed independently of the free node $\mathbf{x} = \varphi(\mathbf{u})$. First, $\mathbf{x}_1 = \varphi(\mathbf{u}_1)$ and $\mathbf{x}_2 = \varphi(\mathbf{u}_2)$ do not

depend on $\mathbf{u}_0 \equiv \mathbf{u}$. Second, by Equations (11) and (12) the image by $\mathbf{T}$ of $\mathbf{x}_1$ and $\mathbf{x}_2$ are also independent on $\mathbf{x}$. In fact:

$$\begin{aligned}\hat{\eta}_{\mathcal{U}}(\mathbf{u}) &= (\hat{\eta} \circ \mathbf{T} \circ \varphi)(\mathbf{u}) = \eta(\mathbf{T}(\varphi(\mathbf{u})), \mathbf{y}_1, \mathbf{y}_2) \\ &= \eta(\mathbf{T}(\varphi(\mathbf{u})), \mathbf{T}(\mathbf{x}_1), \mathbf{T}(\mathbf{x}_2)) = \eta(\tilde{\mathbf{T}}(\varphi(\mathbf{u}), \mathbf{x}_1, \mathbf{x}_2)) \quad (34) \\ &= \eta(\tilde{\mathbf{T}}(\tilde{\varphi}(\mathbf{u}, \mathbf{u}_1, \mathbf{u}_2))) = \eta_{\mathcal{U}}(\mathbf{u}, \mathbf{u}_1, \mathbf{u}_2).\end{aligned}$$

Thus, Equation (34) proves that $\hat{\eta}_{\mathcal{U}}(\mathbf{u})$ and $\eta_{\mathcal{U}}(\mathbf{u}, \mathbf{u}_1, \mathbf{u}_2)$ are equivalent when $\mathbf{u}_1$ and $\mathbf{u}_2$ are fixed.

B Selection of the untangling parameter δ

The modification of the objective function by means of σ_δ, see Equation (28), is sensitive to the selection of the δ parameter. To determine the right value of parameter δ we have to consider the value of σ. On the one hand, δ has to be large enough to ensure that δ^2 is significant compared to σ^2. On the other hand, it has to be small enough to ensure a small perturbation of the location of the minimum of the objective function. It is important to point out that $\delta \neq 0$ is only considered for tangled configurations during the untangling process. Once the minimization of the modified distortion measure has driven the free node inside the feasible region, we use the standard distortion measure to obtain the minimum.

In order to simplify the computation of the derivatives of the distortion measure, at each step of the optimization process, we select a constant value of δ for each submesh. In particular, if the submesh is composed by m triangles, we determine δ taking into account the initial value of σ for all the elements in the submesh: σ_k^*, for $k = 1, \ldots, m$. We propose to use the modified distortion measure only if there is an invalid triangle in the analyzed submesh. That is, if the submesh contains an element with $\sigma_k^* \leq 0$. Moreover, we define $\sigma^* = \min_{k=1,\ldots,m}(\sigma_k^*)$ and we use it to control undesired numerical cancellations in the expression of $\sigma_\delta(\sigma^*)$, see Equation (28). These numerical cancellations appear in triangle configurations where $\sigma^* \ll 0$ and $0 < \delta \ll 1$ because $(\sigma^*)^2 + 4\delta^2 \approx (\sigma^*)^2$, and therefore $\sigma_\delta(\sigma^*) \approx 0$.

To deduce an expression to compute the value of δ, we propose to select the lowest value of δ that ensures that $\sigma_\delta(\sigma^*)$ is numerically always positive. Therefore, we impose

$$\sigma_\delta(\sigma^*) = \frac{1}{2}\left(\sigma^* + \sqrt{(\sigma^*)^2 + 4\delta^2}\right) = \tau > 0, \quad (35)$$

being τ a given tolerance. Hence,

$$\delta(\sigma^*) = \frac{1}{2}\sqrt{(2\ \tau + |\sigma^*|)^2 - (\sigma^*)^2} = \sqrt{\tau^2 + \tau\ |\sigma^*|}. \quad (36)$$

Parameter τ should be a significantly small value compared to the magnitude of σ, but it can not be zero. Therefore, we propose to select

$$\tau = \alpha\ |\sigma^*|, \quad (37)$$

where $\alpha \in [10^{-3}, 10^{-6}]$. Finally, using (37) in (36) we get the final expression for δ:

$$\delta(\sigma^*) = |\sigma^*|\ \sqrt{\alpha^2 + \alpha}. \quad (38)$$

Note that with the presented development, we control that (see Figure 17):

$$\sigma_{\delta(\sigma^*)}(0) = \delta(\sigma^*),$$
$$\sigma_{\delta(\sigma^*)}(\sigma^*) = \tau.$$

In this work, we have selected $\alpha = 10^{-3}$. This value has shown empirically to remove the vertical asymptotes and to slightly modify the location of the distortion minima.

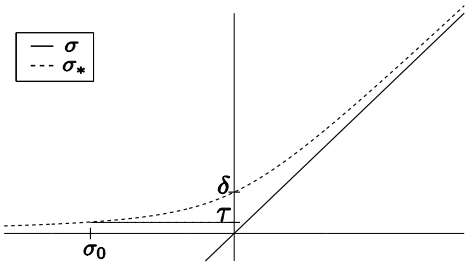

Fig. 17 Representation of $\sigma_\delta(\sigma)$.

C Derivatives of the objective function on parametric coordinates

In this Appendix we deduce the analytical expressions of the first and second order derivatives of the objective function presented in Equation (26). We symbolically denote by α and β the derivative with respect to the parametric variables, u or v.

First and second order derivatives of $\hat{f}$ and $\hat{\eta}_{\mathcal{U}}$

$$\begin{aligned}\frac{\partial \hat{f}}{\partial \alpha} &= 2\sum_{k=1}^{m}(\hat{\eta}_{\mathcal{U}}^k - 1)\ \frac{\partial \hat{\eta}_{\mathcal{U}}^k}{\partial \alpha}, \\ \frac{\partial^2 \hat{f}}{\partial \alpha \partial \beta} &= 2\sum_{k=1}^{m}\left(\frac{\partial \hat{\eta}_{\mathcal{U}}^k}{\partial \alpha}\frac{\partial \hat{\eta}_{\mathcal{U}}^k}{\partial \beta} + (\hat{\eta}_{\mathcal{U}}^k - 1)\ \frac{\partial^2 \hat{\eta}_{\mathcal{U}}^k}{\partial \alpha \partial \beta}\right), \\ \frac{\partial \hat{\eta}_{\mathcal{U}}}{\partial \alpha} &= \frac{\partial(\hat{\eta} \circ \mathbf{T} \circ \varphi)}{\partial \alpha} = D\hat{\eta}\ D\mathbf{T}\ \frac{\partial \varphi}{\partial \alpha}, \\ \frac{\partial^2 \hat{\eta}_{\mathcal{U}}}{\partial \alpha \partial \beta} &= \left(\hat{\eta}_{ac}\mathbf{T}_b^c\varphi_\beta^b\right)\mathbf{T}_b^a\varphi_\alpha^b + \hat{\eta}_a\left(\mathbf{T}_{bc}^a\varphi_\beta^c\right)\varphi_\alpha^b + \hat{\eta}_a\mathbf{T}_b^a\varphi_{\alpha\beta}^b,\end{aligned}$$

where $\mathbf{f}_{bc}^a$ denotes the derivative with respect to variable b and c of the component a of function $\mathbf{f}$.

First and second order derivatives of $\mathbf{T}$

$$\frac{\partial T}{\partial \alpha}(\mathbf{x}) = \frac{\partial \mathbf{M}}{\partial \alpha}(\mathbf{x})\ (\mathbf{x} - \mathbf{x}_1) + \mathbf{M}(\mathbf{x})\ \mathbb{I}_\alpha,$$

where $\mathbb{I}_\alpha$ is the zero vector with a 1 value on coordinate α.

We introduce definitions $\mathbf{e}_2^{\mathrm{p}} := \mathbf{e}_2 - (\mathbf{e}_2^T\ \tilde{\mathbf{e}}_1)\tilde{\mathbf{e}}_1$ and $\mathbb{D} := \det(\tilde{\mathbf{e}}_1, \tilde{\mathbf{e}}_{2,0}, \mathbf{n})$:

$$
\begin{aligned}
\frac{\partial \mathbf{M}}{\partial \alpha} &= \begin{pmatrix} \mathbf{0} & \frac{\partial \tilde{\mathbf{e}}_2}{\partial \alpha} \end{pmatrix}^T, \\
\frac{\partial \tilde{\mathbf{e}}_2}{\partial \alpha} &= \frac{\partial \gamma}{\partial \alpha}\ \tilde{\mathbf{e}}_{2,0} + \gamma\ \frac{\partial}{\partial \alpha}\tilde{\mathbf{e}}_{2,0}, \\
\frac{\partial \gamma}{\partial \alpha} &= \frac{\partial \mathbb{D}}{\partial \alpha}\ \frac{1}{|\mathbb{D}|} + \mathbb{D}\ \frac{\partial}{\partial \alpha}\frac{1}{|\mathbb{D}|}, \\
\frac{\partial}{\partial \alpha}\frac{1}{|\mathbb{D}|} &= -\frac{\pm 1}{|\mathbb{D}|^2}\ \frac{\partial \mathbb{D}}{\partial \alpha}, \\
\frac{\partial}{\partial \alpha}\mathbb{D} &= (\mathbf{n} \times \tilde{\mathbf{e}}_1)\ \frac{\partial}{\partial \alpha}\tilde{\mathbf{e}}_{2,0}, \\
\frac{\partial}{\partial \alpha}\tilde{\mathbf{e}}_{2,0} &= \frac{1}{\|\mathbf{e}_2^{\mathrm{p}}\|}\frac{\partial \mathbf{e}_2^{\mathrm{p}}}{\partial \alpha} + \mathbf{e}_2^{\mathrm{p}}\frac{\partial}{\partial \alpha}\frac{1}{\|\mathbf{e}_2^{\mathrm{p}}\|}, \\
\frac{\partial}{\partial \alpha}\frac{1}{\|\mathbf{e}_2^{\mathrm{p}}\|} &= -\frac{1}{\|\mathbf{e}_2^{\mathrm{p}}\|^3}\left((\mathbf{e}_2^{\mathrm{p}})^T\ \frac{\partial \mathbf{e}_2^{\mathrm{p}}}{\partial \alpha}\right), \\
\frac{\partial}{\partial \alpha}\mathbf{e}_2^{\mathrm{p}} &= \mathbb{I}_\alpha - \tilde{\mathbf{e}}_1^\alpha \tilde{\mathbf{e}}_1, \\
\frac{\partial^2 T}{\partial \alpha \partial \beta}(\mathbf{x}) &= \frac{\partial \mathbf{M}}{\partial \beta}(\mathbf{x})\ \mathbb{I}_\alpha + \frac{\partial \mathbf{M}}{\partial \alpha}(\mathbf{x})\ \mathbb{I}_\beta + \frac{\partial^2 \mathbf{M}}{\partial \alpha \partial \beta}(\mathbf{x})\ (\mathbf{x} - \mathbf{x}_1), \\
\frac{\partial^2 \mathbf{M}}{\partial \alpha \partial \beta} &= \begin{pmatrix} \mathbf{0} & \frac{\partial^2 \tilde{\mathbf{e}}_2}{\partial \alpha \partial \beta} \end{pmatrix}^T, \\
\frac{\partial^2 \tilde{\mathbf{e}}_2}{\partial \alpha \partial \beta} &= \frac{\partial^2 \tilde{\mathbf{e}}_{2,0}}{\partial \alpha \partial \beta}\ \gamma + \frac{\partial \tilde{\mathbf{e}}_{2,0}}{\partial \alpha}\ \frac{\partial \gamma}{\partial \beta} + \\
&\quad \frac{\partial \tilde{\mathbf{e}}_{2,0}}{\partial \beta}\ \frac{\partial \gamma}{\partial \alpha} + \tilde{\mathbf{e}}_{2,0}\ \frac{\partial^2 \gamma}{\partial \alpha \partial \beta}, \\
\frac{\partial^2 \gamma}{\partial \alpha \partial \beta} &= \frac{\partial^2 \mathbb{D}}{\partial \alpha \partial \beta}\ \frac{1}{|\mathbb{D}|} + \frac{\partial \mathbb{D}}{\partial \alpha}\frac{\partial}{\partial \beta}\frac{1}{|\mathbb{D}|} + \\
&\quad \frac{\partial \mathbb{D}}{\partial \alpha}\frac{\partial}{\partial \beta}\frac{1}{|\mathbb{D}|} + \mathbb{D}\frac{\partial^2}{\partial \alpha \partial \beta}\frac{1}{|\mathbb{D}|}, \\
\frac{\partial^2}{\partial \alpha \partial \beta}\frac{1}{|\mathbb{D}|} &= \frac{2}{|\mathbb{D}|^3}\frac{\partial \mathbb{D}}{\partial \alpha}\frac{\partial \mathbb{D}}{\partial \beta} - \frac{\pm 1}{|\mathbb{D}|^2}\frac{\partial^2 \mathbb{D}}{\partial \alpha \partial \beta}, \\
\frac{\partial^2}{\partial \alpha \partial \beta}\mathbb{D} &= \frac{1}{\|\mathbf{e}_2^{\mathrm{p}}\|}\ \frac{\partial^2 \mathbf{e}_2^{\mathrm{p}}}{\partial \alpha \partial \beta} + \frac{\partial \|\mathbf{e}_2^{\mathrm{p}}\|^{-1}}{\partial \beta}\ \frac{\partial \mathbf{e}_2^{\mathrm{p}}}{\partial \alpha} + \\
&\quad \frac{\partial \mathbf{e}_2^{\mathrm{p}}}{\partial \beta}\ \frac{\partial \|\mathbf{e}_2^{\mathrm{p}}\|^{-1}}{\partial \alpha} + \mathbf{e}_2^{\mathrm{p}}\ \frac{\partial^2 \|\mathbf{e}_2^{\mathrm{p}}\|^{-1}}{\partial \alpha \partial \beta}, \\
\frac{\partial^2}{\partial \alpha \partial \beta}\frac{1}{\|\mathbf{e}_2^{\mathrm{p}}\|} &= \frac{2}{\|\mathbf{e}_2^{\mathrm{p}}\|^3}\frac{\partial}{\partial \beta}\|\mathbf{e}_2^{\mathrm{p}}\|\ \frac{\partial}{\partial \alpha}\|\mathbf{e}_2^{\mathrm{p}}\| - \frac{1}{\|\mathbf{e}_2^{\mathrm{p}}\|^2}\frac{\partial^2}{\partial \alpha \partial \beta}\|\mathbf{e}_2^{\mathrm{p}}\|, \\
\frac{\partial^2}{\partial \alpha \partial \beta}\|\mathbf{e}_2^{\mathrm{p}}\| &= \frac{\partial}{\partial \beta}\tilde{\mathbf{e}}_{2,0}\ \frac{\partial}{\partial \alpha}\mathbf{e}_2^{\mathrm{p}}, \text{ since } \frac{\partial^2 \mathbf{e}_2^{\mathrm{p}}}{\partial \alpha \partial \beta} = 0.
\end{aligned}
$$

First and second order derivatives of $\hat{\eta}$

$$
\begin{aligned}
\frac{\partial \hat{\eta}_{ss}}{\partial \alpha} &= \frac{\partial \hat{\eta}_{sh}}{\partial \alpha}\ \hat{\eta}_{si} + \hat{\eta}_{sh}\ \frac{\partial \hat{\eta}_{si}}{\partial \alpha}, \\
\frac{\partial \hat{\eta}_{sh}}{\partial \alpha} &= 2\hat{\eta}_{sh}\ \left(\frac{\left(\frac{\partial \mathbf{S}}{\partial \alpha}, \mathbf{S}\right)}{|\mathbf{S}|^2} - \frac{\frac{\partial \sigma}{\partial \alpha}}{2\sqrt{\sigma^2 + 4\delta^2}}\right), \\
\frac{\partial \sigma}{\partial \alpha} &= \sigma\ \mathrm{tr}\left(\mathbf{S}^{-1}\frac{\partial \mathbf{S}}{\partial \alpha}\right), \text{ see [14]}, \\
\frac{\partial \mathbf{S}}{\partial \alpha} &= \frac{\partial \mathbf{A}}{\partial \alpha}\ \mathbf{W}^{-1}, \\
\frac{\partial \mathbf{A}}{\partial x} &= \begin{pmatrix} -1 & -1 \\ 0 & 0 \end{pmatrix}, \quad \frac{\partial \mathbf{A}}{\partial y} = \begin{pmatrix} 0 & 0 \\ -1 & -1 \end{pmatrix}, \\
\frac{\partial \hat{\eta}_{si}}{\partial \alpha} &= -\mu_*^{-2}\ \frac{\partial \mu_*}{\partial \sigma}\ \frac{\partial \sigma}{\partial \alpha}, \\
\frac{\partial \mu_*}{\partial \sigma} &= \frac{\mathrm{e}}{2}\ \left(\mathrm{e}^{-\sigma} - \sigma \mathrm{e}^{-\sigma} - \frac{1}{\sigma^2}\mathrm{e}^{-\frac{1}{\sigma}} + \frac{1}{\sigma^3}\mathrm{e}^{-\frac{1}{\sigma}}\right), \\
\frac{\partial^2 \hat{\eta}_{ss}}{\partial \alpha \partial \beta} &= \frac{\partial^2 \hat{\eta}_{sh}}{\partial \alpha \partial \beta}\eta_{si} + \frac{\partial \hat{\eta}_{sh}}{\partial \alpha}\frac{\partial \hat{\eta}_{si}}{\partial \beta} + \\
&\quad \frac{\partial \hat{\eta}_{sh}}{\partial \beta}\frac{\partial \hat{\eta}_{si}}{\partial \alpha} + \hat{\eta}_{sh}\frac{\partial^2 \hat{\eta}_{si}}{\partial \alpha \partial \beta}, \\
\frac{\partial^2 \hat{\eta}_{sh}}{\partial \alpha \partial \beta} &= \frac{\partial^2 (\mathbf{S}, \mathbf{S})}{\partial \alpha \partial \beta}\frac{1}{2\sigma_\delta} + \frac{\partial (\mathbf{S}, \mathbf{S})}{\partial \alpha}\frac{\partial}{\partial \beta}\frac{1}{2\sigma_\delta} + \\
&\quad \frac{\partial (\mathbf{S}, \mathbf{S})}{\partial \beta}\frac{\partial}{\partial \alpha}\frac{1}{2\sigma_\delta} + (\mathbf{S}, \mathbf{S})\frac{\partial^2}{\partial \alpha \partial \beta}\frac{1}{2\sigma_\delta}, \\
\frac{\partial^2 (\mathbf{S}, \mathbf{S})}{\partial \alpha \partial \beta} &= 2(\frac{\partial \mathbf{S}}{\partial \alpha}, \frac{\partial \mathbf{S}}{\partial \beta}), \\
\frac{\partial^2}{\partial \alpha \partial \beta}\frac{1}{2\sigma_\delta} &= \frac{1}{\sigma_\delta^3}\frac{\partial \sigma_\delta}{\partial \beta}\frac{\partial \sigma_\delta}{\partial \alpha} - \frac{1}{2\sigma_\delta^2}\frac{\partial^2 \sigma_\delta}{\partial \alpha \partial \beta}, \\
\frac{\partial^2 \sigma_\delta}{\partial \alpha \partial \beta} &= \frac{2\delta^2}{(\sigma^2(\mathbf{S}) + 4\delta^2)^{3/2}}\frac{\partial \sigma(\mathbf{S})}{\partial \beta}\frac{\partial \sigma(\mathbf{S})}{\partial \alpha}, \\
\frac{\partial^2 \hat{\eta}_{si}}{\partial \alpha \partial \beta} &= 2\mu_*^{-3}\left(\frac{\partial \mu_*}{\partial \sigma}\right)^2\frac{\partial \sigma}{\partial \alpha}\frac{\partial \sigma}{\partial \beta} - \\
&\quad \mu_*^{-2}\frac{\partial^2 \mu_*}{\partial \sigma^2}\frac{\partial \sigma}{\partial \alpha}\frac{\partial \sigma}{\partial \beta} - \mu_*^{-2}\frac{\partial \mu_*}{\partial \sigma}\frac{\partial^2 \sigma}{\partial \alpha \partial \beta}, \\
\frac{\partial^2 \mu_*}{\partial \sigma^2} &= \frac{\mathrm{e}}{2}\ \left(-2\mathrm{e}^{-\sigma} + \sigma \mathrm{e}^{-\sigma} + \frac{2\mathrm{e}^{-\frac{1}{\sigma}}}{\sigma^3} - \frac{4\mathrm{e}^{-\frac{1}{\sigma}}}{\sigma^4} + \frac{1\mathrm{e}^{-\frac{1}{\sigma}}}{\sigma^5}\right).
\end{aligned}
$$

References

1. Alliez, P., Ucelli, G., Gotsman, C., Attene, M.: Recent Advances in Remeshing of Surfaces. Tech. rep., EU network of excellence (2005)
2. Alliez, P., de Verdire, E.C., Devillers, O., Isenburg, M.: Isotropic surface remeshing. In: Shape Modeling International, 2003, pp. 49–58 (2003)
3. Do Carmo, M.: Differential Geometry of Curves and Surfaces. Prentice-Hall, Inc., Englewood Cliffs, New Jersey (1976)
4. Escobar, J.M., Montenegro, R., Rodríguez, E., Montero, G.: Simultaneous aligning and smoothing of surface triangulations. Engrg. Comput. **27**(1), 17–29 (2011)
5. Escobar, J.M., Montero, G., Montenegro, R., Rodríguez, E.: An algebraic method for smoothing surface triangulations on a local parametric space. Int. J. Numer. Methods Engrg. **66**(4), 740–760 (2006)
6. Escobar, J.M., Rodríguez, E., Montenegro, R., Montero, G., González-Yuste, J.M.: Simultaneous untangling and smoothing of tetrahedral meshes. Comput. Methods Appl. Mech. Engrg. **192**(25), 2775–2787 (2003)

7. Field, D.: Qualitative measures for initial meshes. Int. J. Numer. Methods Engrg. **47**(4), 887–906 (2000)
8. Freitag, L.A., Knupp, P.M.: Tetrahedral mesh improvement via optimization of the element condition number. Int. J. Numer. Methods Engrg. **53**, 1377–1391 (2002)
9. Freitag, L.A., Plassmann, P.: Local optimization-based simplicial mesh untangling and improvement. Int. J. Numer. Methods Engrg. **49**, 109–125 (2000)
10. Frey, P.J., Borouchaki, H.: Geometric surface mesh optimization. Comput. Visual. Sci. **1**(3), 113–121 (1998)
11. Garimella, R., Shashkov, M.: Polygonal surface mesh optimization. Engrg. Comput. **20**(3), 265–272 (2004)
12. Garimella, R., Shashkov, M., Knupp, P.M.: Triangular and quadrilateral surface mesh quality optimization using local parametrization. Comput. Methods Appl. Mech. Engrg. **193**(9–11), 913–928 (2004)
13. Giuliani, S.: An algorithm for continuous rezoning of the hydrodynamic grid in arbitrary lagrangian-eulerian computer codes. Nucl. Engrg. Des. **72**(2), 205–212 (1982)
14. Golberg, M.: The derivative of a determinant. Amer. Math. Monthly **79**(10), 1124–1126 (1972)
15. Herrmann, L.: Laplacian-isoparametric grid generation scheme. J. Engrg. Mech. Div. **102**(5), 749–756 (1976)
16. Jiao, X., Wang, D., Zha, H.: Simple and effective variational optimization of surface and volume triangulations. Engrg. Comput. **27**, 81–94 (2011)
17. Knupp, P.M.: Algebraic mesh quality metrics. SIAM J. Numer. Anal. **23**(1), 193–218 (2001)
18. Knupp, P.M.: Hexahedral and tetrahedral mesh untangling. Engrg. Comput. **17**(3), 261–268 (2001)
19. Knupp, P.M.: Algebraic mesh quality metrics for unstructured initial meshes. Finite Elem. Anal. Des. **39**(3), 217–241 (2003)
20. Knupp, P.M.: A method for hexahedral mesh shape optimization. Int. J. Numer. Methods Engrg. **58**(2), 319–332 (2003)
21. Leng, J., Zhang, Y., Xu, G.: A novel geometric flow-driven approach for quality improvement of segmented tetrahedral meshes. In: Proc. 20th Int. Meshing Roundtable, pp. 347–364 (2012)
22. Liu, L., Tai, C., Ji, Z., Wang, G.: Non-iterative approach for global mesh optimization. Computer-Aided Design **39**(9), 772–782 (2007)
23. López, E.J., Nigro, N.M., Storti, M.A.: Simultaneous untangling and smoothing of moving grids. Int. J. Numer. Methods Engrg. **76**(7), 994–1019 (2008)
24. Mullen, P., Tong, Y., Alliez, P., Desbrun, M.: Spectral Conformal Parameterization. Comput. Graph. Forum **27**(5), 1487–1494 (2008)
25. Nocedal, J., Wright, S.: Numerical optimization. Springer verlag (1999)
26. Roca, X.: Paving the path towards automatic hexahedral mesh generation. Ph.D. thesis, Universitat Politècnica de Catalunya (2009)
27. Roca, X., Gargallo-Peiró, A., Sarrate, J.: Defining quality measures for high-order planar triangles and curved mesh generation. In: Proc. 20th Int. Meshing Roundtable, pp. 365–383. Springer Berlin Heidelberg (2012)
28. Roca, X., Ruiz-Gironés, E., Sarrate, J.: ez4u: Mesh generation environment. www-lacan.upc.edu/ez4u.htm (2010)
29. Roca, X., Sarrate, J., Ruiz-Gironés, E.: Congreso de métodos numéricos y computacionales en ingeniería, semni. In: Communications in Numerical Methods in Engineering. Porto (2007)
30. Shivanna, K., Grosland, N., Magnotta, V.: An analytical framework for quadrilateral surface mesh improvement with an underlying triangulated surface definition. In: Proc. 19th International Meshing Roundtable, pp. 85–102. Chattanooga (2010)
31. Vartziotis, D., Athanasiadis, T., Goudas, I., Wipper, J.: Mesh smoothing using the geometric element transformation method. Comput. Methods Appl. Mech. Engrg. **197**, 3760–3767 (2008)
32. Zhang, Y., Bajaj, C., Xu, G.: Surface smoothing and quality improvement of quadrilateral/hexahedral meshes with geometric flow. Communications in Numerical Methods in Engineering **25**(1), 1–18 (2009)

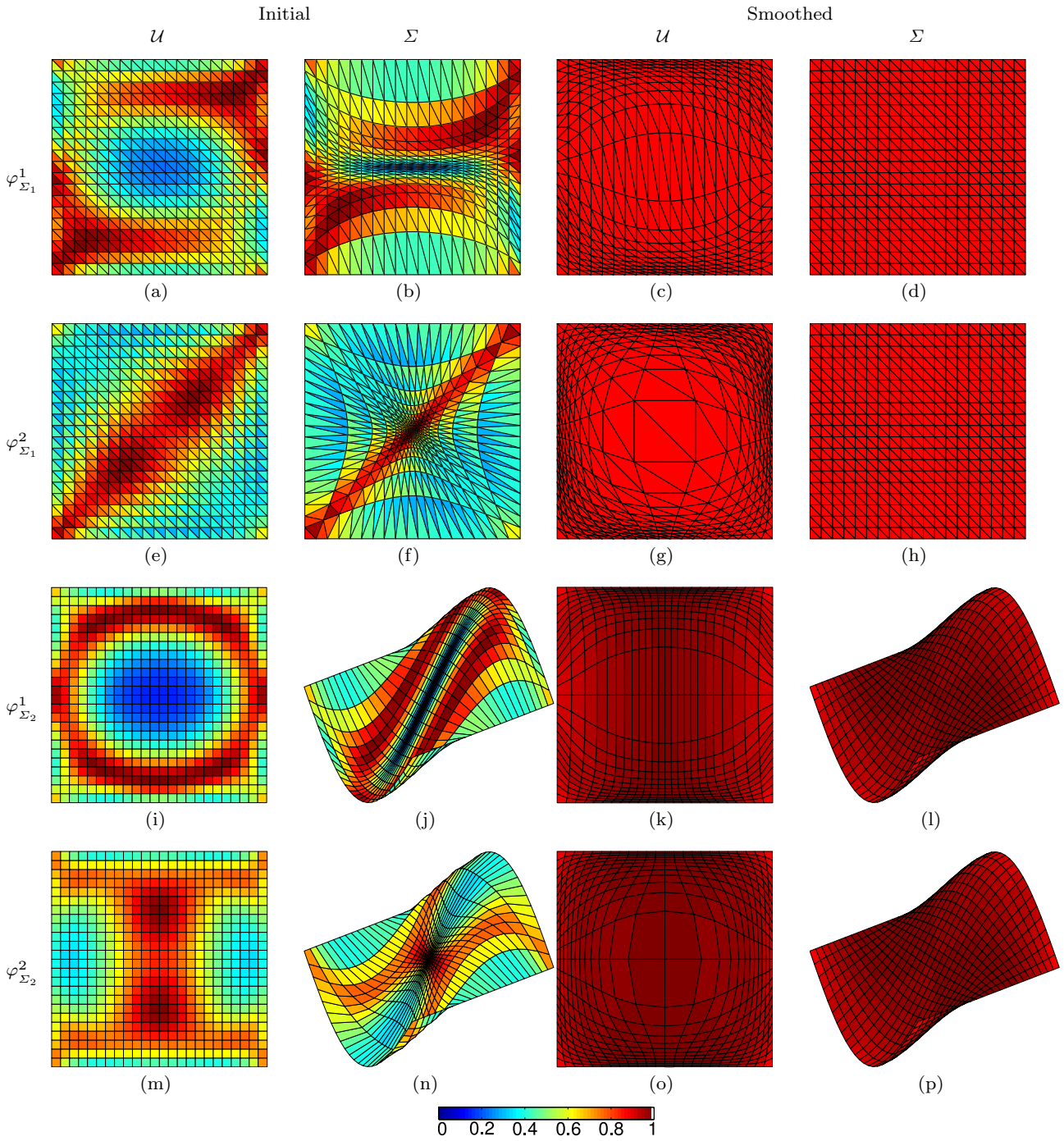

Fig. 8 Independence of the optimization procedure on the surface parameterization. Meshes on Σ_1 parameterized by $\varphi^1_{\Sigma_1}$: (a,b) initial meshes on $\mathcal{U}^1_{\Sigma_1}$ and on Σ_1; (c,d) smoothed meshes on $\mathcal{U}^1_{\Sigma_1}$ and on Σ_1. Meshes on Σ_1 parameterized by $\varphi^2_{\Sigma_1}$: (e,f) initial meshes; (g,h) smoothed meshes. Meshes on Σ_2 parameterized by $\varphi^1_{\Sigma_2}$: (i,j) initial meshes; (k,l) smoothed meshes. Meshes on Σ_2 parameterized by $\varphi^2_{\Sigma_2}$: (m,n) initial meshes; (o,p) smoothed meshes. All meshes colored according to the shape quality measure.

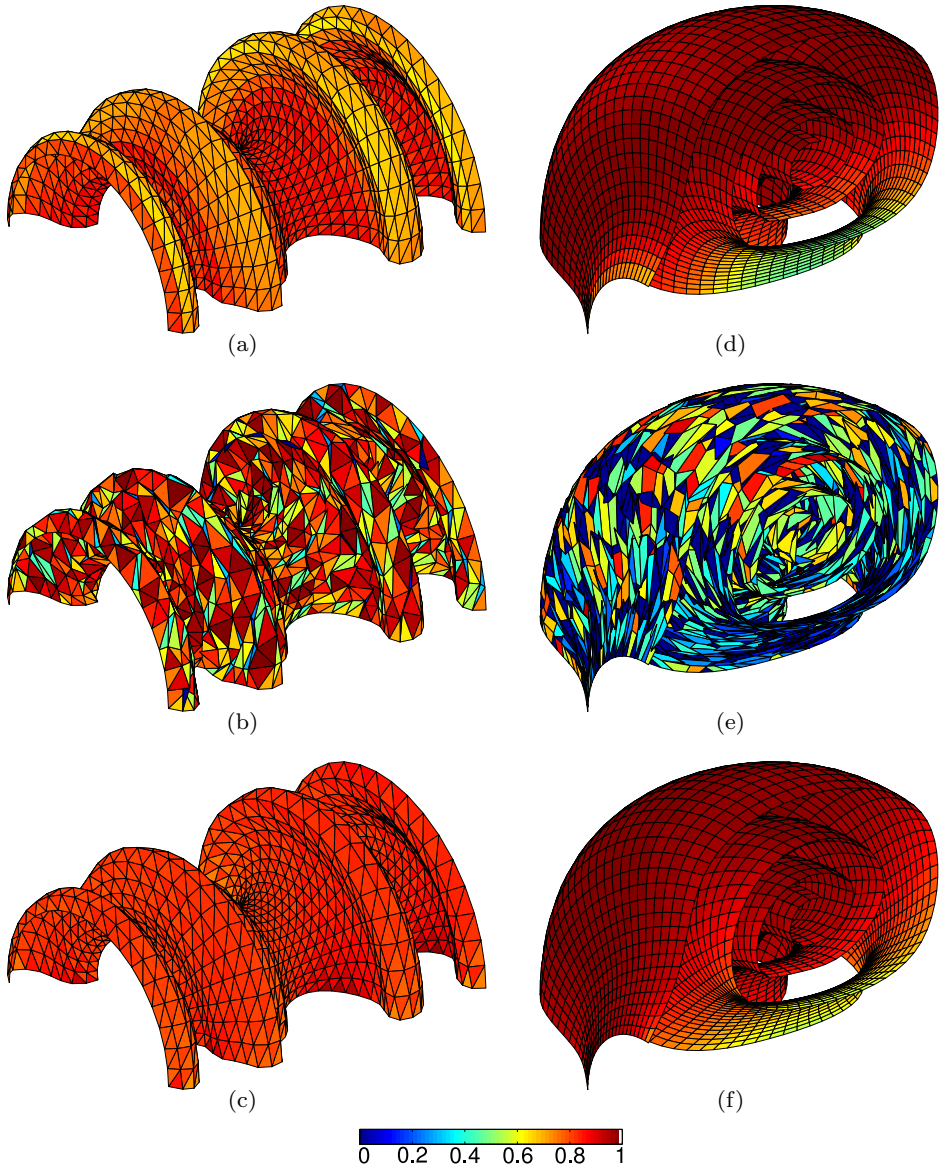

Fig. 9 Meshes colored according to the shape quality measure for a revolution surface: (a) initial mesh, (b) tangled mesh, and (c) smoothed and untangled mesh. Meshes colored according to the shape quality measure for a rolled surface, (d) initial mesh, (e) tangled mesh, and (f) smoothed and untangled mesh.

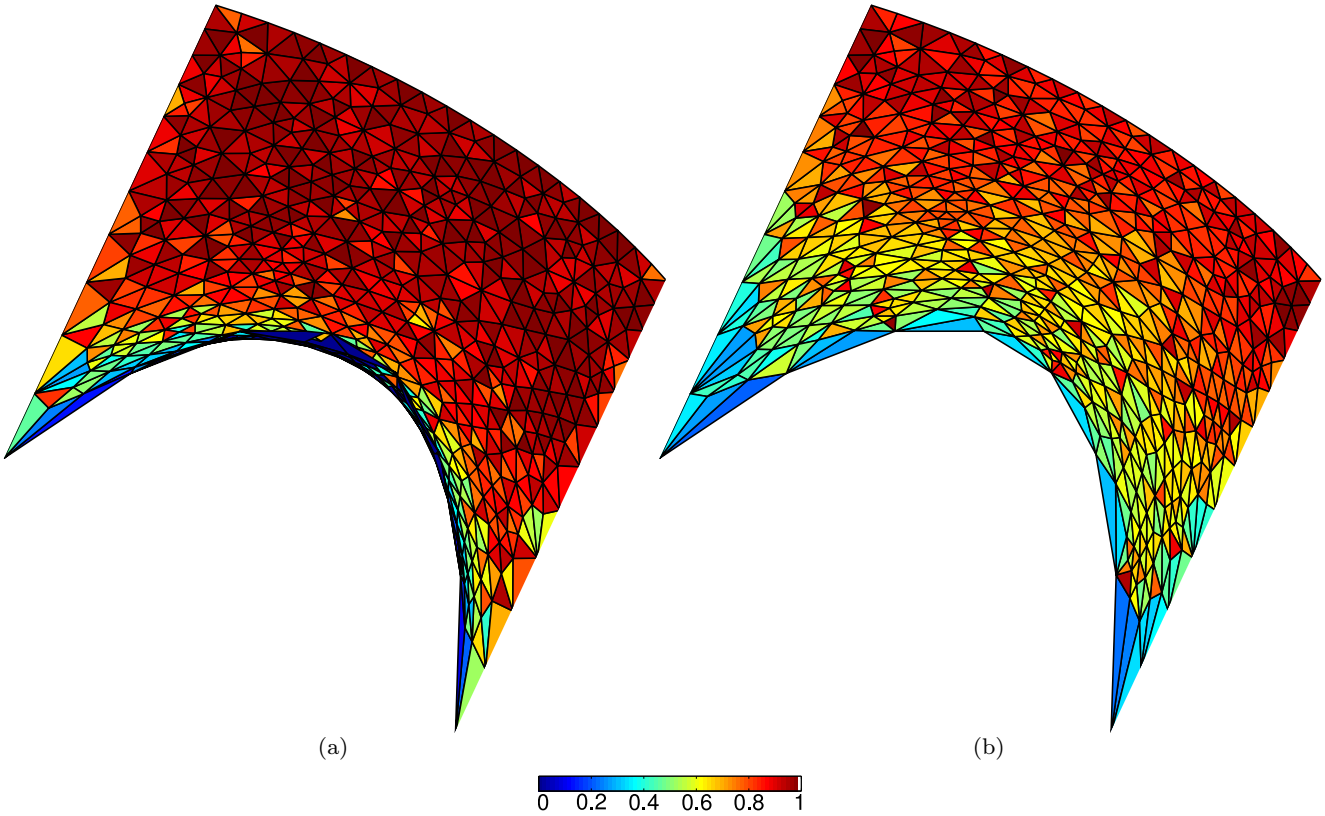

Fig. 10 Smoothed meshes on a cylinder using (a) Laplacian smoothing, and (b) minimization of the shape distortion measure.

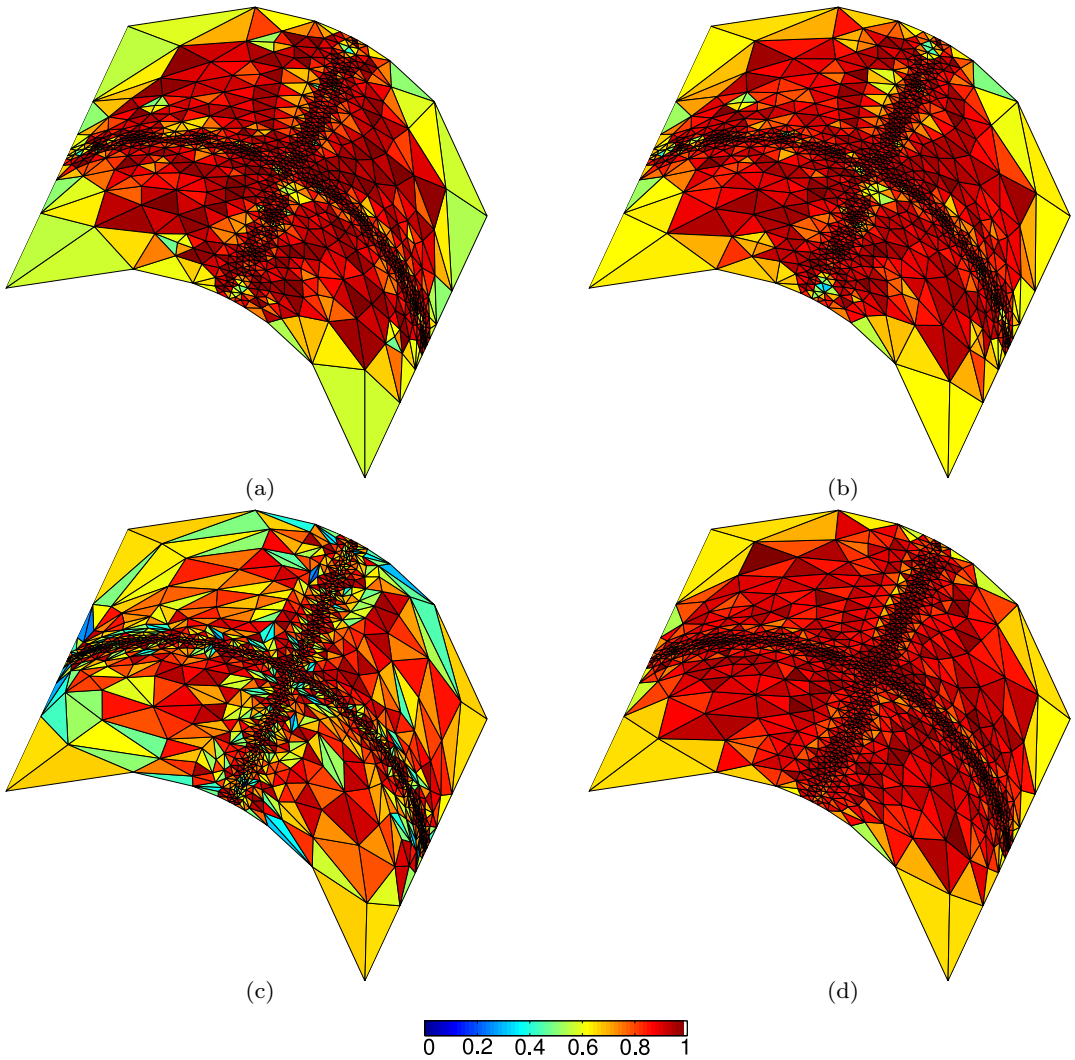

Fig. 12 Surface triangular meshes on a cylinder colored according to the size-shape quality measure. (a) Initial mesh. Smoothed meshes using (b) shape, (c) size and (d) size-shape distortion measures, respectively.

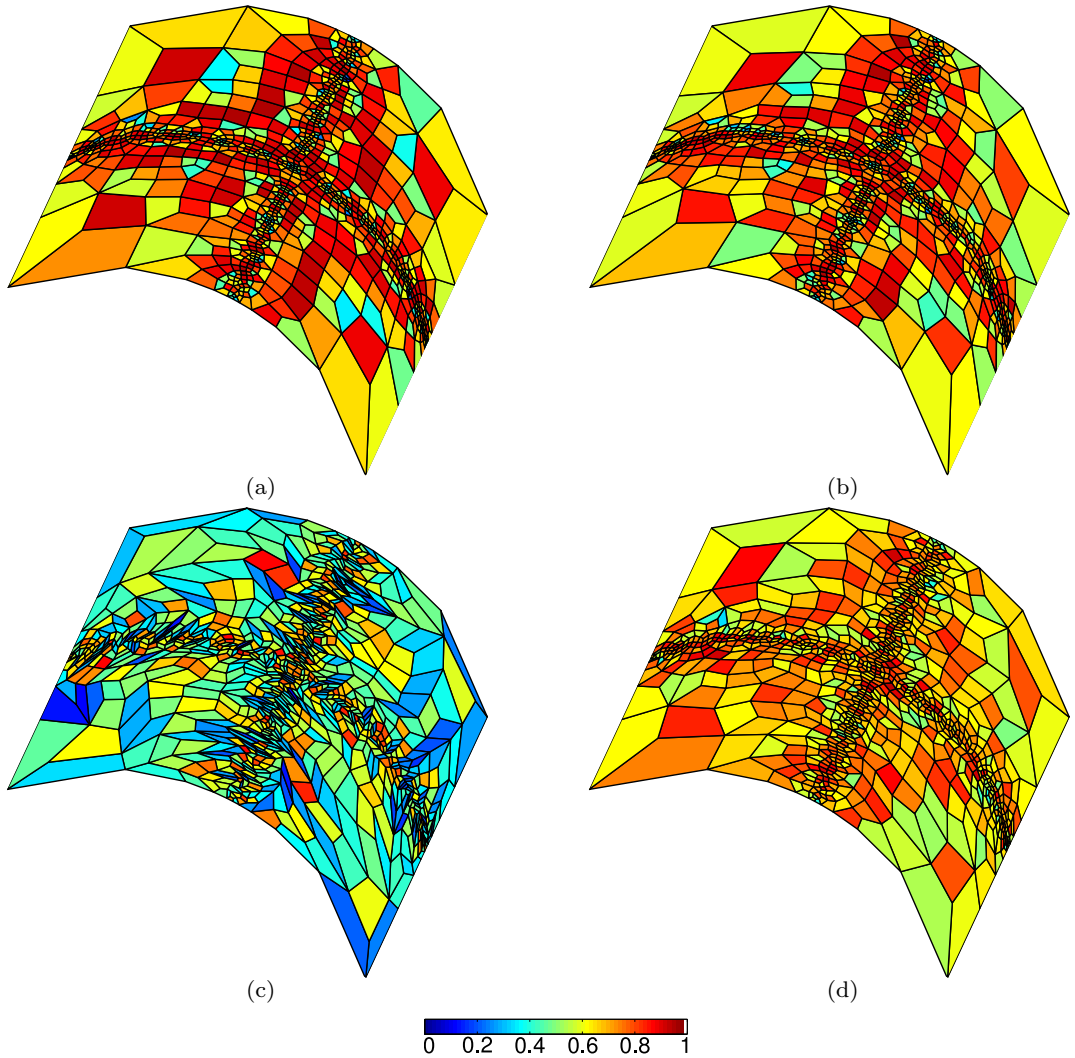

Fig. 13 Surface quadrilateral meshes on a cylinder colored according to the size-shape quality measure. (a) Initial mesh. Smoothed meshes using (b) shape, (c) size and (d) size-shape distortion measures, respectively.

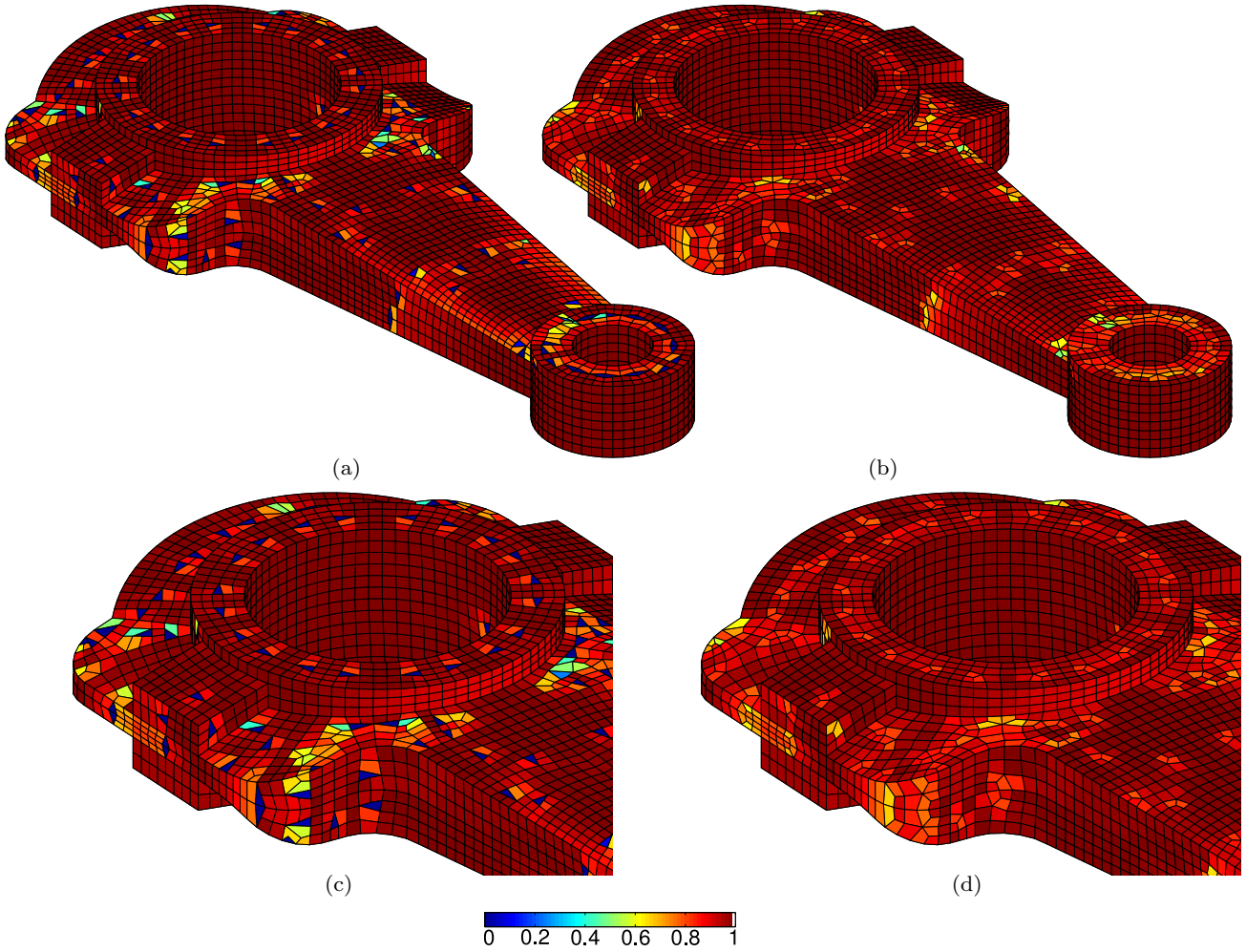

Fig. 14 Quadrilateral meshes colored according to the shape quality measure on a linking rod: (a) initial mesh, (b) smoothed mesh, (c) detail of the initial mesh, and (d) detail of the smoothed mesh.

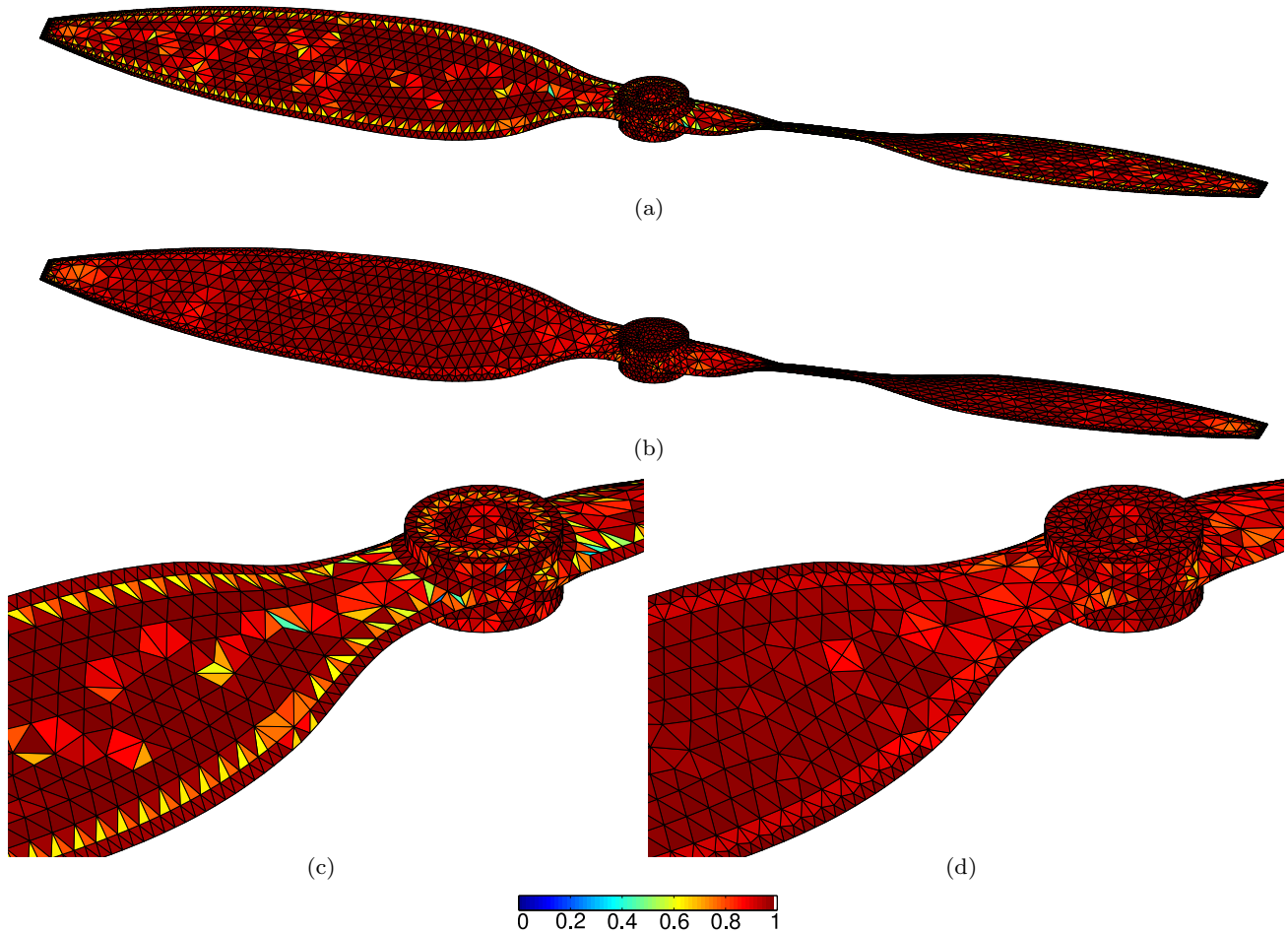

Fig. 15 Triangular meshes colored according to the shape quality measure on a propeller: (a) initial mesh; (b) smoothed mesh; (c) detail of the initial mesh, and (d) detail of the smoothed mesh.

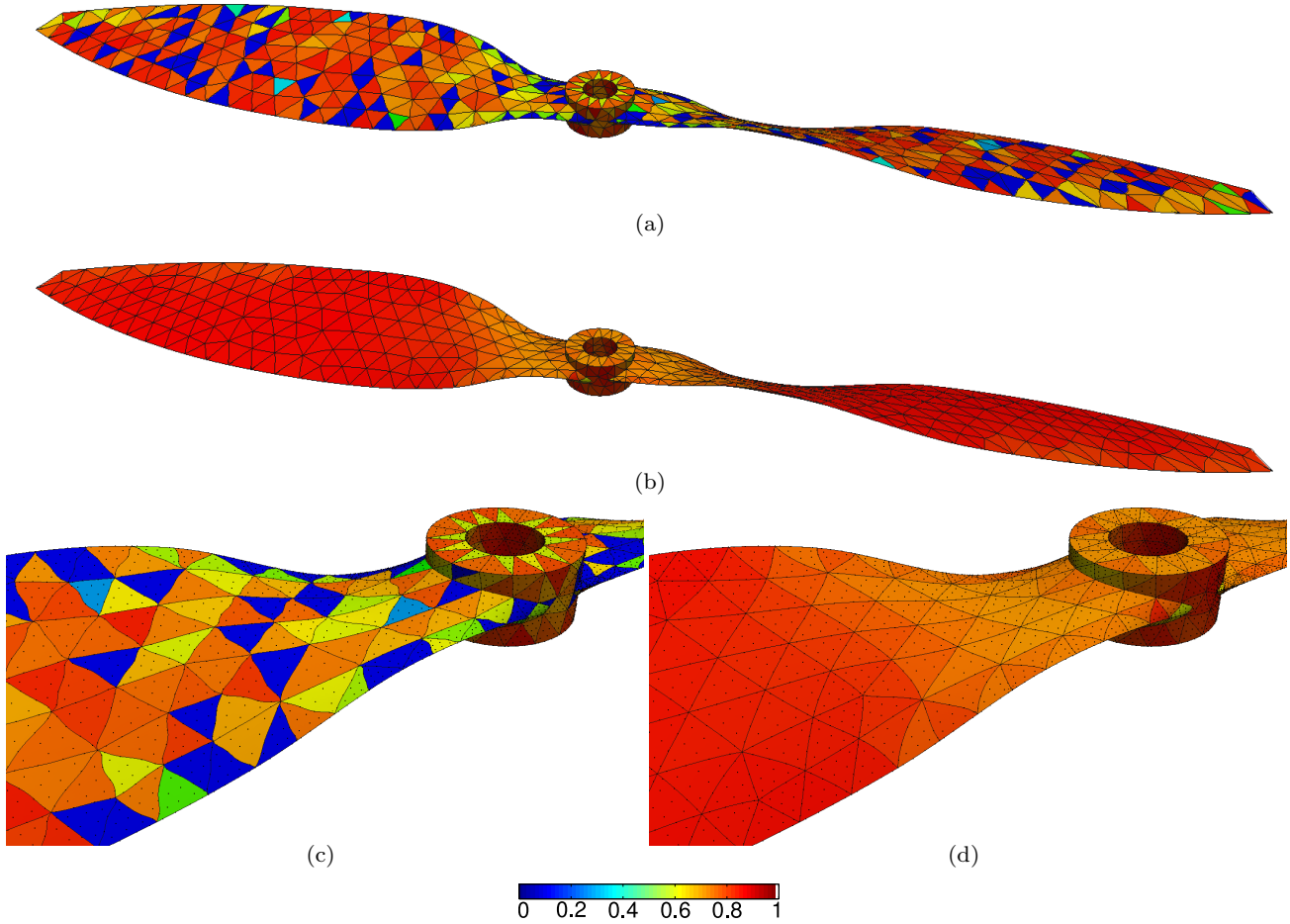

Fig. 16 Triangular meshes of interpolation degree five colored according to the shape quality measure on a propeller: (a) initial mesh; (b) smoothed mesh; (c) detail of the initial mesh, and (d) detail of the smoothed mesh.